HHS Public Access

Author manuscript

Brain Res. Author manuscript; available in PMC 2016 October 14.

Published in final edited form as:

Brain Res. 2015 October 14; 1623: 174–192. doi:10.1016/j.brainres.2015.04.044.

High-resolution *in vivo* optical imaging of stroke injury and repair

Sava Sakadžić[a,*], **Jonghwan Lee**[a], **David A. Boas**[a], and **Cenk Ayata**[b,c]

[a]Optics Division, MHG/MIT/HMS Athinoula A Martinos Center for Biomedical Imaging, Department of Radiology, Massachusetts General Hospital and Harvard Medical School, Charlestown, MA 02129, USA

[b]Neurovascular Research Laboratory, Department of Radiology, Massachusetts General Hospital and Harvard Medical School, Charlestown, MA 02129, USA

[c]Stroke Service and Neuroscience Intensive Care Unit, Department of Neurology, Massachusetts General Hospital and Harvard Medical School, Boston, MA 02114, USA

Abstract

Central nervous system (CNS) function and dysfunction are best understood within a framework of interactions between neuronal, glial and vascular compartments comprising the neurovascular unit (NVU), all of which contribute to stroke-induced CNS injury, plasticity, repair, and recovery. Recent advances in *in vivo* optical microscopy have enabled us to observe and interrogate cells and their processes with high spatial resolution in real time and in their natural environment deep in the brain tissue. Here, we review some of these state-of-the-art imaging techniques with an emphasis on imaging the interactions among the constituents of the NVU during ischemic injury and repair in small animal models.

1. Introduction

Brain injury, whether ischemic, hemorrhagic or traumatic, is a significant cause of morbidity and mortality, and a major socioeconomic burden. Prevention of brain injury and its acute to subacute progression, and facilitating the repair and recovery processes are among the highest priorities in translational neuroscience with the ultimate goal of improving functional outcome. Decades of research has raised our awareness to the fact that individual cells and cell types in the brain do not react to injury alone. Rather, cells work as part of an ensemble (e.g., neurovascular unit) and interact with and react to each other through cell-cell communications that can be electrical, chemical or even mechanical. Indeed, not only does each cell type reacts to injury in different ways, but the same cell type (e.g., microglia) can have two or more faces and change its phenotype at different stages of injury evolution. An improved understanding of this complex cellular and molecular response to injury is needed

*Corresponding author (sava.sakadzic@mgh.harvard.edu).

in order to guide interventions that suppress those processes that are perceived as harmful and enhance those that are perceived as beneficial after injury. In the context of injury progression and subsequent mechanisms of repair, phenotypic changes in each cell type, and specific interactions between cells of the same or different types, will no doubt be better understood if structural and functional changes are visualized at a cellular level. Today, we are closer than ever to achieving this goal, owing in part to recent technological advances in high-resolution *in vivo* optical imaging that can observe and interrogate cells and even their processes in real time in their natural environment, thereby preserving the complex ensemble. As such, *in vivo* imaging is anticipated to provide clinically relevant data on the spatiotemporal patterns of tissue injury and repair processes, help improve interventional therapies, and lead to the discovery of novel markers of recovery as well as selective targeted therapies.

Historically, optical imaging has been a major tool for investigating the physiological processes from a subcellular scale to entire organs, owing to its unique properties such as high temporal and spatial resolution within reasonable thicknesses of tissue, numerous contrast mechanisms, and modest cost of instrumentation. Traditional optical microscopy techniques such as widefield or confocal microscopy imaging are not capable of penetrating more than several tens of micrometers into the optically highly scattering brain tissue, which significantly limits *in vivo* applications. Recently, high-spatial resolution optical imaging technologies capable of penetrating up to one millimeter into the tissue have been developed and applied to *in vivo* brain imaging. In this article we review these state-of-the-art imaging techniques with an emphasis on high-resolution imaging of stroke injury and repair in rodents.

Several important characteristics of the imaging modality are critical to assess cells in their natural environment during stroke: 1) ability to image the same region of interest longitudinally, *in vivo;* 2) high spatial resolution, sufficient to resolve individual cells, capillaries, or even subcellular structures such as dendritic spines and axonal boutons; 3) high temporal resolution, sufficient to resolve the time course of dynamic cellular processes; 4) penetration depth of at least several hundred micrometers into the tissue, to enable imaging of several cortical layers; and 5) high specificity and sensitivity to various structural and functional imaging parameters.

Only a few optical microscopy technologies satisfy these requirements and have been applied to image ischemic stroke in rodents, such as multi-photon laser scanning microscopy (MPM), optical coherence tomography (OCT), and photoacoustic imaging (PAI). Among these, MPM imaging is the most mature and widely applied (Helmchen and Denk, 2005; Svoboda and Yasuda, 2006). In typical MPM applications to *in vivo* brain imaging, it is common to achieve ∼500 μm penetration depth, ∼1 μm spatial resolution, and a few microseconds temporal resolution per voxel. The MPM detects photoluminescence (e.g. fluorescence, phosphorescence) that comes from endogenous or exogenous chromophores, and images are typically created from the sequences of sequential point measurements. Brain imaging with MPM can be performed through thinned skull in mice (Drew et al., 2010), although more commonly a glass-covered cranial window is used to increase the penetration depth. In addition to MPM, recent advances in OCT and PAI have led to

important demonstrations of their utility in high resolution *in vivo* brain studies. OCT is usually described as an optical analog of ultrasonic pulse-echo imaging (Drexler and Fujimoto, 2008). OCT detects optical scattering from within the tissue to form cross sectional images, and, therefore, does not require exogenous contrast agents. Spatial resolution in common OCT setups ranges from ∼1 μm to a few tens of micrometers. The signal reflected from multiple locations along the optical axis of the system (A-scans) can be acquired simultaneously, which gives a significant speed advantage to OCT over MPM in volumetric imaging. The typical penetration depth in rodent brain is ∼1 mm (Srinivasan et al., 2012a). Lastly, PAI is a hybrid technology that forms images by listening to ultrasonic waves generated by thermoelastic tissue expansion (Wang and Gao, 2014; Yao and Wang, 2014). PAI's contrast mechanism comes from the optical absorption of the excitation light by chromophores of endogenous or exogenous origin, thereby creating heat (Li et al., 2007; Yao and Wang, 2014). The high resolution applications of PAI rely on tight optical focusing of excitation light (optical-resolution photoacoustic microscopy, OR-PAM) (Maslov et al., 2008) and can achieve several micrometers spatial resolution with ∼1 mm penetration depth in a rodent brain (Hu et al., 2009; Wang et al., 2013a). The detection of ultrasonic waves in OR-PAM allows rapid acquisition of A-scans and, analogous to OCT, generation of three-dimensional images from two-dimensional scans.

Below, we first review the structural and then the functional imaging applications of these technologies. Non-imaging optical techniques can also be used to manipulate the structure of function of the tissue in stroke research, such as microstrokes induced by using high-energy laser pulses (Foerch et al., 2013; Nishimura et al., 2006), vessel occlusion by optically activating Rose Bengal photosensitizer (Watson et al., 1985; Zhang et al., 2005), optogenetics (Cheng et al., 2014), and glutamate uncaging (Noguchi et al., 2011). However, such tools are beyond the scope of this manuscript.

2. Cellular morphology

Various optical techniques can achieve cellular spatial resolution at the brain surface, but their penetration depth is typically limited to only a few tens of micrometers, which limits the scope of their *in vivo* applications. The development of MPM (Denk et al., 1990) has enabled fast cellular and subcellular resolution imaging in brain tissue with penetration depths of up to several hundreds of micrometers (Svoboda and Yasuda, 2006). Over the past couple of decades MPM has emerged as the most versatile tool for imaging cellular morphology *in vivo*. Only recently have other optical microscopy technologies for deep tissue imaging (i. e., optical coherence tomography and photoacoustic microscopy) been applied for the same purpose. In this section we review the current imaging capabilities for deep *in vivo* assessment of brain tissue cellular morphology.

2.1 Neurons

Fluorescent proteins (XFPs) and fluorescent dyes have been developed for MPM imaging to target specific cell populations in the brain. The green fluorescent protein (GFP) (Chalfie et al., 1994), numerous mutants of GFP, and many XFPs from other species have been used to create a number of fusion proteins and biosensors that can tag proteins and enzymes in cells and label specific populations of cells (Chudakov et al., 2010). XFPs are generally suitable

for MPM imaging and offer additional advantages of specificity and simplicity of experimental preparation (since they are already present in the cells), brightness, and relative resistance to photo bleaching (Giepmans et al., 2006). Advanced neuronal labeling such as the brainbow toolbox are continuously improved for applications in the rodent brain (Cai et al., 2013), and efforts to extend XFPs emission to higher wavelengths and to enable deeper imaging are intensifying (Kremers et al., 2011; Shcherbakova and Verkhusha, 2013). Today, an extensive arsenal of tools for neuronal labeling with XFPs is available to study brain injury and repair *in vivo* (Canty et al., 2013; Feng et al., 2000; Hartmann et al., 2014; Li and Murphy, 2008; Mascaro et al., 2013; Sigler and Murphy, 2010). In addition, numerous 'traditional' dyes (Giepmans et al., 2006) and combinations of dye molecules attached to proteins (O'Hare et al., 2007) are available. The very high spatial resolution of MPM permits mapping of individual neurons and their connections, and monitoring of dendritic spine and axonal bouton dynamics (Svoboda et al., 1997) in response to pathological stimuli, *in vivo* (Li and Murphy, 2008; Zhang et al., 2005; Zhang and Murphy, 2007). For example, MPM imaging of neuronal morphology during ischemia/reperfusion in mice (Fig. 1A and B) revealed various degrees of structural damage and recovery across the focal ischemic territory over time, with spatial heterogeneity ranging from severely and irreversibly damaged core to reversibly damaged penumbra to structurally intact areas within microdomains (Li and Murphy, 2008).

Optical coherence microscopy (OCM) provides label-free high resolution imaging of neurons. Cortical neuronal cell bodies and myelinated axons in rats are clearly visible in OCM images down to one millimeter depth (Srinivasan et al., 2012a). Sensitivity to axons is somewhat diminished when their orientation is parallel with the optical axis and sensitivity to glial cells seems to be significantly lower than to neurons. Label-free dynamic light scattering-optical coherence tomography (DLS-OCT) can also visualize individual neurons and it can assess intracellular motility as has been shown in the rat cortex during ischemic stroke (Lee et al., 2013a) (Fig. 1C). Interestingly, neuronal cell bodies can be identified both structurally (low backscattering as revealed in OCM) and dynamically (intracellular organelle motions in DLS-OCT). Intracellular motility was significantly reduced both during 1-hour middle cerebral artery occlusion (MCAO) and after reperfusion. As such, OCM can be a sensitive and specific tool to assess tissue viability, density of axons and neuronal cell bodies, and potentially for monitoring the myelination changes in longitudinal studies of brain injury, such as after chronic mild forebrain hypoperfusion or in hypertensive animal models.

2.2 Glial, vascular, and stem cells

Glial MPM imaging was widely popularized owing to the red fluorescent dye Sulforhodamine 101 (SR101) (Nimmerjahn et al., 2004), which labels astrocytes and mature myelinating oligodendrocytes upon topical application (Hill and Grutzendler, 2014). Advances in XFPs and the further development of fluorescent dyes resulted in a large pool of fluorescent labels than can selectively target astrocytes, microglia, and oligodendrocytes with high specificity (Bardehle et al., 2013; Davalos et al., 2005; Hughes et al., 2013; Milner, 2012; Nimmerjahn et al., 2005; Sword et al., 2013). In a study by Davalos et al. (2005), a response of GFP-expressing microglia to traumatic brain injury in hetero-zygous

C×3cr1$^{GFP/+}$ mice was imaged by MPM. The experiments have shown that ATP release from a localized cortical traumatic injury site induced a rapid response from parenchymal microglia, where their processes created a barrier between the healthy and injured tissue (Fig. 2A). Recent study by Bardehle et al. (2013) utilized eGFP-expressing astrocytes in GLAST/eGFP mice and revealed that astrocytic proliferation in response to a localized cortical injury is limited only to juxtavascular astrocytes in proximity of the injury site (Fig. 2B). Finally, Huges et al. (2013) have shown that eGFP-expressing oligodendrocyte precursor cells (NG2+ cells) in NG2-meGFP mice are highly dynamic, actively exploring their cortical territory. In response to a focal injury, NG2+ cells are slowly migrating towards the injury site over many days while continuously maintaining their density by proliferation (Fig. 2C).

In addition, significantly improved labeling of cells that comprise the building blocks of the microvasculature has been achieved. Several advanced labeling strategies based on XFPs are available for tagging smooth muscle cells and pericytes (Armulik et al., 2011; Hall et al., 2014; Iliff et al., 2013; Milesi et al., 2014; Thrane et al., 2013). Understanding the role of pericytes in microvascular blood flow control is critically important for understanding regulation of resting CBF and functional hyperemia (Hall et al., 2014), as well as cerebral ischemia and reperfusion (Yemisci et al., 2009). In a study by Milesi et al. (2014), mice expressing DsRed fluorescent protein under NG2 promoter (Zhu et al., 2008) were used to quantify the NG2-DsRed perivascular ramifications after status epilepticus (SE) (Fig. 3B). Using NG2 promoter results in labeling several cell types in the brain (e.g. oligodendrocyte precursor cells, pericytes) (Nishiyama et al., 2009), which are commonly differentiated in *in vivo* experiments based on their morphology and proximity to the vasculature. Endothelial cells can also be visualized using XFPs (Iliff et al., 2014; Knowland et al., 2014; Lam et al., 2010) in addition to more traditional fluorescent labeling such as Rhodamine 6G and lectin (Michalski et al., 2010; Niklass et al., 2014). For example, MPM imaging of GFP expressing endothelial cells in Tie2-GFP mice (Lam et al., 2010) revealed a novel mechanism of vessel wall plasticity involved in microvascular recanalization after microembolic occlusion (Fig. 3A). In another study (Knowland et al., 2014), mice with endothelial tight junctions labeled by eGFP were imaged by MPM to show that transcellular impairment of the blood brain barrier (BBB) due to focal ischemia precedes the paracellular BBB impairment (Fig. 3C).

Optical-resolution photoacoustic microscopy has potential to image various cellular constituents based on their absorption, such as DNA and RNA in nuclei (D.-K. Yao et al., 2010), cytochromes (Zhang et al., 2013), and myelin (Matthews et al., 2014). This enables label-free monitoring of cell viability, demyelination, and, potentially, cellular metabolism via assessment of the ratio of reduced to oxidized cytochromes. However, since these measurements rely on illumination of the tissue with the short-wavelength visible and ultraviolet light, their applications may be limited to the superficial cortical layers.

3. Local brain tissue hemodynamic and metabolic parameters

Quantitative *in vivo* cellular-level resolution measurement of various inorganic molecules (e.g. Na^+, Zn^{2+}, O_2, K^+, Ca^{2+}, H_2O_2, NO, Cl^-, O_2^-, H^+), small and large biomolecules (e.g. glucose (Glc), nicotinamide adenine dinucleotide (NAD^+), Flavin adenine dinucleotide

(FAD), adenosine triphosphate (ATP), matrix metalloproteinases (MMPs), nitric oxide synthases (NOSs), superoxide dismutases (SODs), phospholipases (PLAs), cyclooxygenases (COXs)), as well as local blood flow and metabolism represent a largely unmet need in stroke research. Cellular interactions at the site of brain injury are strongly influenced by local tissue metabolic state. Therefore, simultaneous monitoring of local hemodynamic and metabolic parameters, including cerebral blood flow and intravascular and tissue oxygenation, is critical for understanding the cascade of cellular events during acute injury and repair.

3.1 Blood Flow

MPM is often used for high-resolution measurements of microvascular dynamics in small animal models (Kleinfeld et al., 1998; Shih et al., 2012) (Fig. 4A). The technique enables depth-resolved measurements of vessel diameters and RBC flux and velocities (Kamoun et al., 2010; Kleinfeld et al., 1998). MPM utilizes fluorescent labeling of either plasma or RBCs and track the RBCs speed and flux in individual microvessels, including the capillaries. Imaging is typically performed through a sealed cranial window, although thin skull preparation is also a viable option in cases where reduced penetration depth is acceptable (Drew et al., 2010). Using commonly available MPM setups, vessel diameters and RBC movement can be routinely measured through a sealed cranial window down to ∼500 μm depth from the cortical surface (Shih et al., 2012). There is a tradeoff between the number of simultaneously monitored vessels and temporal resolution. Fast blood flow transients (<1 s) can be continuously monitored in only a few vessel segments at a time, while all vessels in the field of view can be sampled with ∼12 s temporal resolution (Kamoun et al., 2010). Vascular measurements with MPM has been instrumental in studying ischemic stroke damage to dendrites and their spines as a function of blood flow changes at the microvascular scales (Zhang and Murphy, 2007). Acute ischemic damage to dendrites was triggered within 30 min when hypoperfused cortical area was >0.2 mm^2. A remarkably sharp transition between intact and damaged synaptic circuitry occurred over tens of μm and was defined by a transition between perfused and occluded vessels (Fig. 1B). In a group of studies addressing the reorganization of blood flow following local disruption of the microvascular network (i.e. targeted ‘microstrokes’) (Nishimura et al., 2010, 2007, 2006; Schaffer et al., 2006), MPM imaging of blood flow was utilized to map the adaptation of microvascular blood flow patterns in response to individual vessel occlusion (Fig. 4A). Since collateral flow between neighboring penetrating arterioles is limited, occlusion of a penetrating arteriole has a devastating effect on the flow through downstream microvessels, unlike pial arterioles and the capillary network.

Optical Coherence Tomography (OCT) enables depth-resolved imaging of absolute blood flow in individual cortical arterioles and venules as well as measurements of the RBC flux in capillaries (Bouwens et al., 2013; Lee et al., 2014, 2013b; Liu et al., 2013; Srinivasan et al., 2012b, 2010a, 2009; Tokayer et al., 2013; Wang et al., 2007; Wang and An, 2009; Wang and Wang, 2010; Weiss et al., 2013) (Figs. 4B,C and 5). Compared to MPM measurements of blood flow, advantages of OCT include increased penetration depth through thinned skull in mice and >1 mm penetration depth through a cranial window, reliance on endogenous contrast (i.e. optical scattering) instead of exogenous contrast agents, and improved

acquisition speed. OCT measurements of the absolute cortical blood flow have been validated (Srinivasan et al., 2011) and full volumetric imaging of blood flow over a cortical surface area of 1 mm^2 is possible in ~1 minute (Srinivasan et al., 2010b). In a study by Srinivasan et al. (2013), OCT was utilized in acute stroke in mice to access multiple microscopic biomarkers for eventual infarction, including capillary non-perfusion, cerebral blood flow deficiency, altered cellular scattering, and impaired autoregulation of cerebral blood flow. Longitudinal monitoring revealed vascular remodeling and flow recovery one week after chronic stroke. In addition to CBF measurements in non-capillary vessels, significant progress was made in quantitative OCT measurement of capillary blood flow (Lee et al., 2014, 2013b; Srinivasan et al., 2012b). Volumetric images of capillary RBC flux can be obtained in a few minutes (Fig. 4 C and D), opening the possibilities to study capillary perfusion in brain ischemia and reperfusion models (Lee et al., 2013b). In combination with MPM, this technology will enable studying the influence of pericytes and immune responses to brain injury at a capillary level. Commercial systems are also available, facilitating widespread adoption of OCT. However, the data analysis for the OCT blood flow measurements is significantly more complex than for the MPM flow measurements. Therefore, widespread adoption of OCT flow measurements may also require availability of sophisticated data processing toolboxes. In short, while OCT has only recently emerged as a tool for studying brain injury (Jia et al., 2009; Ren et al., 2012; Shen et al., 2014; Srinivasan et al., 2013), we expect its importance to grow rapidly and complement the measurements afforded by MPM.

Several ‘flavors’ of photoacoustic imaging (PAI) have been developed to optimize spatial resolution and penetration depth, and to enhance sensitivity to different tissue functional and metabolic parameters (Wang and Gao, 2014; Wang and Hu, 2012). Although PAI is mostly utilized for quantitative imaging of total hemoglobin concentration and oxygenation in the cerebral microvasculature, blood flow can be measured with PAI as well. By utilizing this technology, characteristics of cerebral blood flow can be measured using several different approaches, including blood velocity measurement in arterioles and venules based on Doppler broadening of the ultrasonic bandwidth (J. Yao et al., 2010), combining ultrasonic thermal tagging with photoacoustic imaging (Wang et al., 2013b), and even single RBC velocity measurement (Wang et al., 2013a). A combination of PAI measurements of cortical blood flow and oxygen saturation is particularly attractive for investigation of brain pathology since it may provide an estimate of the absolute cerebral metabolic rate of oxygen (CMRO2).

3.2 Microvascular and tissue oxygenation

MPM can be utilized to measure absolute oxygen concentration with cellular resolution in both brain tissue and blood plasma (Finikova et al., 2008; Sakadžić et al., 2010; Lecoq et al., 2011) (Fig. 6). The technique is based on phosphorescence lifetime imaging of oxygen (PLIO2), which measures oxygen-dependent phosphorescence lifetimes of an exogenous contrast agent (Rumsey et al., 1988; Vanderkooi et al., 1987). The phosphorescence lifetime of a probe depends on the partial pressure of oxygen (PO2) in the immediate vicinity of the probe, providing a spatially localized measurement of dissolved oxygen. Probe molecules for MPM were specially designed for two-photon excitation, with a high degree of

encapsulation that ensures stability of lifetime calibration in a complex biological environment (Finikova et al., 2008; Lebedev et al., 2009; Roussakis et al., 2014). Unlike spectroscopy-based hemoglobin saturation measurements, PLIO2 lifetime imaging is insensitive to changes in tissue optical properties during imaging. The acquisition speed is currently limited to 0.2 to 1 second per measurement point by relatively long phosphorescence lifetimes and the number of decay averages required at each point. Further development of oxygen sensitive dyes with significantly higher quantum yield, two-photon absorption cross section, and dynamic range will enable significant improvements in acquisition speed and precision of PO2 imaging (Esipova and Vinogradov, 2014). The technology was used to obtain high-resolution maps of oxygen concentration distribution in both the microvasculature and tissue under various conditions (Devor et al., 2011; Kazmi et al., 2013; Parpaleix et al., 2013; Sakadžić et al., 2014; Spencer et al., 2014). Since cerebral oxygen delivery, consumption, and reserve in microvascular domains in both normal and diseased brain is largely unknown, we expect that PLIO2 will be an invaluable tool for assessing the relation between blood flow and metabolic perturbations, treatments, and tissue injury during ischemia and reperfusion. Combined PLIO2 and other MPM measurements will enable obtaining critical information about the local oxygenation to support an arsenal of MPM tools for investigations of cell-cell interactions in stroke.

Since hemoglobin is a dominant optical absorber of visible and near-infrared radiation in the brain, photoacoustic imaging (PAI) is ideally suited for quantitative imaging of total hemoglobin concentration and oxygenation in cerebral microvasculature. In particular, high spatial resolution variants of PAI can achieve ∼1 mm penetration depth in the brain and were successfully applied to measure arteriolar, venular and capillary SO2 as well as single RBC oxygenation (Hu et al., 2009; Wang et al., 2013a; Yao and Wang, 2014). Numerous applications related to brain injury and repair were conducted in the last few years, including brain edema after cold injury (Z. Xu et al., 2011), dynamics of the microvascular oxygenation after middle cerebral artery occlusion (Hu et al., 2011) and during epileptic seizure (Tsytsarev et al., 2013) (Fig. 6). The ability of PAI to longitudinally measure RBC oxygen saturation and flux in capillaries will allow studying capillary flow dynamics in stroke and, potentially, measuring local CMRO2 confined to individual microvascular territories.

Another imaging technique - visible light OCT (vis-OCT) – is emerging as an alternative technology that may provide rapid noninvasive measurements of the microvascular oxygenation in the future (Robles et al., 2011; Yi et al., 2014; Chong et al., 2015). This will expand existing set of OCT tools for measurements of blood flow, cellular morphology and viability to include critically important measurements of oxygen extraction and CMRO2.

3.3 NADH

Nicotinamide adenine dinucleotide (NAD) is an important coenzyme for energy metabolism, and the reduced form (NADH) is intrinsically fluorescent (for recent reviews see (Heikal, 2010; Shuttleworth, 2010; Turner et al., 2007)). Relative NADH fluorescence intensity changes can be imaged using both single-photon excitation (Harbig et al., 1976) and multi-photon excitation (Baraghis et al., 2011; Huang et al., 2002; Kasischke et al., 2011, 2004)

and can serve as an indicator of the rate of oxidative phosphorylation. In addition to relative NADH fluorescence intensity imaging, the measurement of NADH fluorescence lifetimes may provide insight into the different bound states of NADH and consequently provide more quantitative assessment of energy metabolism (Vishwasrao et al., 2005; Yaseen et al., 2013). Multi-photon imaging of relative NADH fluorescence intensity changes has been applied *in vivo* in healthy cerebral cortex (Kasischke et al., 2011) and during experimentally induced cortical spreading depression (Takano et al., 2007; Yuzawa et al., 2012) (Fig. 6C). These studies indicate that cortical spreading depression (CSD) in mice causes a transient increase in O2 demand exceeding vascular O2 supply.

Numerous genetically encoded fluorescent sensors are now being developed (San Martín et al., 2014b; Zhang et al., 2014), including sensors for monitoring intracellular NADH levels (Bilan et al., 2014; Hung et al., 2011; Hung and Yellen, 2014; Zhao et al., 2011). These sensors may provide stronger signal than endogenous NADH fluorescence and may enable *in vivo* imaging of NADH cellular compartmentalization as well as features inaccessible by traditional NADH fluorescence imaging such as measurement of NAD^+/NADH ratio. NAD^+/NADH ratio reflects overall redox state of the cell and it may provide critical information about cellular metabolism at various degrees of tissue ischemia, during normal or pathological brain activation (e.g., spreading depolarizations), and in response to treatments.

3.4 Glucose

Fluorescent glucose analogs, such as 6-deoxy-N-(7-nitrobenz-2-oxa-1,3-diazol-4-yl)-aminoglucose (6-NBDG) or 2-NBDG can be utilized to estimate glucose transport deep into brain cortex with high resolution *in vivo* using either multi-photon microscopy (Chuquet et al., 2010) or photoacoustic microscopy (Yao et al., 2013). However, transport kinetics of individual glucose transporters significantly differ between glucose and fluorescent glucose analogs (Barros et al., 2009), as well as between neuronal and glial cells (Simpson et al., 2007), making data interpretation challenging. In addition, measurements utilizing fluorescent glucose analogs require accumulation of the glucose analog over minutes, which is not optimal for studying fast metabolic transients such as periinfarct depolarizations, epileptic seizures, or functional activation. Further advances in the design of novel glucose probes or glucose fluorescent sensors may address these challenges (Lee et al., 2011; Klonoff, 2012; Pickup et al., 2013, 2005).

3.5 ATP, Glutamate, Pyruvate, and Lactate

Genetically encoded nanosensors (San Martín et al., 2014b; Zhang et al., 2014) show great promise for high resolution absolute quantification of previously inaccessible molecules involved in brain energy metabolism, such as ATP (Berg et al., 2009; Imamura et al., 2009; Liemburg-Apers et al., 2011; Tantama et al., 2013), glutamate (Borghuis et al., 2013; Marvin et al., 2013; Okumoto et al., 2005), pyruvate (San Martín et al., 2014a), and lactate (San Martín et al., 2013). Since the majority of these novel probes are based on fluorescent proteins, they are potentially suitable for high resolution *in vivo* multiphoton imaging (Marvin et al., 2013).

4. Ca^{2+} and other cellular functional markers

The development of MPM imaging of Ca^{2+} (Helmchen and Denk, 2005; Svoboda et al., 1997; Svoboda and Yasuda, 2006) has had enormous influence on the investigation of the plethora of diverse neuronal and glial calcium functions (Grienberger and Konnerth, 2012; Kuchibhotla et al., 2009). MPM enables the detection of dendritic calcium signals *in vivo* and can be used to reconstruct spike trains. Chemical (synthetic) Ca^{2+} indicators (Grynkiewicz et al., 1985) such as fura-2 and Oregon Green BAPTA offer high temporal resolution and sensitivity and they were widely applied to brain imaging *in vivo*, including longitudinal studies of functional rewiring and recovery after stroke (Cianchetti et al., 2013; Winship and Murphy, 2008) (Figs. 7 and 8). Endogenous Ca^{2+} sensors based on XFPs provide an elegant solution for some important issues frequently associated with exogenous (synthetic) Ca^{2+} indicators such as the lack of specificity to a particular cellular populations and the lack of control over intracellular localization (Chen et al., 2013; Grienberger and Konnerth, 2012).

In addition to Ca^{2+} imaging, the ability to quantitatively measure numerous other inorganic molecules and biomolecules with high-resolution *in vivo* will revolutionize stroke research. Here we mention some recent progress towards various indicators of cellular function, noting that any *in vivo* applications of these sensors are mostly lacking. Over the years significant progress has been made towards detecting various metal ions (Dean et al., 2012; Penner-Hahn, 2013), including Zn^{2+} (Carter et al., 2011; Guo et al., 2012; Radford et al., 2013; Wang et al., 2011; You et al., 2011), Na^{+} (Schreiner and Rose, 2013), and K^{+} (Padmawar et al., 2005). Probes were also developed for detecting small molecules such as NO (Dong et al., 2013; Yu et al., 2012), H^{+} (pH probes) (Han and Burgess, 2010; Kim et al., 2013), singlet O_2 (Song et al., 2013; K. Xu et al., 2011), H_2O_2 (Belousov et al., 2006; Guo et al., 2014), Cl^{-} (Arosio and Ratto, 2014), large biomolecules such as matrix metalloproteinases (Vandenbroucke and Libert, 2014) and various biothiols (Xu et al., 2014), as well as complex cellular processes such as labeling dying cells with propidium iodide (Driscoll et al., 2011) or assessing the glutathione redox potential (Gutscher et al., 2008).

This long list of functional cellular indicators implies that there is a very significant discrepancy between the tremendous efforts to develop novel chromophores and fluorophores for the detection of various cellular functional markers and their *in vivo* brain imaging applications. High resolution imaging of Ca^{2+} concentration is unique in its highly successful applications to *in vivo* imaging, while reliable measurements of other functional markers such as O_2 concentration are just emerging (please refer to the previous section for O_2 imaging examples). We mention here two important obstacles related to *in vivo* brain imaging, which must be overcome to enable reliable imaging of a cellular functional marker. The first is that interactions of the chromophore with the biological environment must not affect function of the chromophore, i.e. changing its specificity, sensitivity, or any other key measurement parameter. This is typically very difficult to achieve and the majority of optical probes that show a high promise *in vitro* fail in *in vivo* applications. The second obstacle is related to transient changes in tissue optical properties (e.g. scattering and absorption) that are frequently present in *in vivo* applications. These changes are part of

normal physiological or pathological responses induced during the experiment and their influence on the measured signal is typically significant and difficult to remove. Measurements based on photoluminescence lifetimes are an example of a detection scheme that is insensitive to changes in the tissue optical properties and local chromophore concentration (Finikova et al., 2008; Sakadžić et al., 2010). However, the signal in the majority of imaging methods have moderate to significant sensitivity to changes in tissue optical properties and further efforts such as signal correction based on advanced modeling (Baraghis et al., 2011) are needed to enable reliable quantitative measurements.

High-resolution *in vivo* imaging of cellular functional markers in the brain is still dominantly performed by MPM. Photoacoustic imaging is well suited for molecular imaging (Deliolanis et al., 2014; Li et al., 2007), but the penetration depth may be compromised when trying to achieve micrometer-size spatial resolution. Optical coherence tomography also has potential for molecular imaging in the brain *in vivo* (Boustany et al., 2010; Yang, 2005).

5. Future technological developments

Microscopy technologies have been steadily improved for faster and deeper imaging with better spatial resolution and additional functionality. We refer here to reviews and some of the latest technological advances of individual technologies: (Hoover and Squier, 2013; Horton et al., 2013; Kobat et al., 2011; An et al., 2013; Lu et al., 2014; Robles et al., 2011; Wang and Gao, 2014). Of particular interest for stroke studies may be the efforts to miniaturize the optical illumination and signal collection elements of the microscopy systems to enable recordings in awake behaving animals (Sawinski et al., 2009). Also, the combination of two or more imaging modalities such as MPM and OCT (Sakadžićc et al., 2014) and PAI and OCT (Li et al., 2009) will allow simultaneous measurement of multiple relevant physiological and biophysical parameters and the inference of processes that cannot be measured directly.

In addition to MPM, OCT, and PAI, the further development of several novel high-resolution optical imaging technologies and their application to *in vivo* brain imaging may have significant impact on stroke studies. Raman spectroscopy observes vibrational, rotational, and other low-frequency modes and provides a label-free fingerprint by which molecules can be identified with a high sensitivity and chemical specificity (Bowley et al., 1989). This enables identification and quantification of many molecules otherwise inaccessible by other imaging technologies. In particular, experimental setups based on coherent anti-Stokes Raman scattering microscopy may be only a few years away from *in vivo* applications (Camp Jr et al., 2014; Saar et al., 2014; Tu and Boppart, 2014). Super-resolution imaging brakes the optical resolution limits of Abbe's diffraction and enables nanometer-scale spatial resolution suitable for visualization of the tiny perisynaptic processes, radial glia endfeet, endothelial tight junctions, etc. Several different forms of super resolution optical imaging are available such as stimulated emission depletion (STED) (Nägerl et al., 2008; Wildanger et al., 2009; Willig et al., 2006), photo-activation localization (PALM) (Shroff et al., 2001), stochastic optical reconstruction (STORM) (Huang et al., 2008), and total internal reflection (TIRF) (Fish, 2001). These technologies currently have limited depth of penetration and/or long sampling times so they are still

limited to the analysis of cultured cells or fixed tissue. The development of super-resolution imaging techniques for *in vivo-use* will have a tremendous impact on our understanding of the evolution of the brain injury in stroke.

Acknowledgments

The authors would like to thank Kassandra Kisler for useful discussion. We would also like to thank support from the National Institute of Health (grants EB018464, EB000790, NS055104, NS061505 and K99EB014879), Foundation Leducq, the Heitman Foundation, and the Ellison Foundation.

References

An L, Li P, Lan G, Malchow D, Wang RK. High-resolution 1050 nm spectral domain retinal optical coherence tomography at 120kHz A-scan rate with 6.1 mm imaging depth. Biomed Opt Express. 2013; 4:245–259.10.1364/BOE.4.000245 [PubMed: 23411636]

Armulik A, Genové G, Betsholtz C. Pericytes: Developmental, Physiological, and Pathological Perspectives, Problems, and Promises. Dev Cell. 2011; 21:193–215.10.1016/j.devcel.2011.07.001 [PubMed: 21839917]

Arosio D, Ratto GM. Twenty years of fluorescence imaging of intracellular chloride. Front Cell Neurosci. 2014; 8:258.10.3389/fncel.2014.00258 [PubMed: 25221475]

Baraghis E, Devor A, Fang Q, Srinivasan VJ, Wu W, Lesage F, Ayata C, Kasischke KA, Boas DA, Sakadžić S. Two-photon microscopy of cortical NADH fluorescence intensity changes: correcting contamination from the hemodynamic response. J Biomed Opt. 2011; 16:106003–13. 106003. 10.1117/1.3633339 [PubMed: 22029350]

Bardehle S, Krüger M, Buggenthin F, Schwausch J, Ninkovic J, Clevers H, Snippert HJ, Theis FJ, Meyer-Luehmann M, Bechmann I, Dimou L, Götz M. Live imaging of astrocyte responses to acute injury reveals selective juxtavascular proliferation. Nat Neurosci. 2013; 16:580–586.10.1038/nn.3371 [PubMed: 23542688]

Barros LF, Bittner CX, Loaiza A, Ruminot I, Larenas V, Moldenhauer H, Oyarzún C, Alvarez M. Kinetic validation of 6-NBDG as a probe for the glucose transporter GLUT1 in astrocytes. J Neurochem. 2009; 109:94–100.10.1111/j.l471-4159.2009.05885.x [PubMed: 19393014]

Belousov VV, Fradkov AF, Lukyanov KA, Staroverov DB, Shakhbazov KS, Terskikh AV, Lukyanov S. Genetically encoded fluorescent indicator for intracellular hydrogen peroxide. Nat Methods. 2006; 3:281–286.10.1038/nmeth866 [PubMed: 16554833]

Berg J, Hung YP, Yellen G. A genetically encoded fluorescent reporter of ATP:ADP ratio. Nat Methods. 2009; 6:161–166.10.1038/nmeth.l288 [PubMed: 19122669]

Bilan DS, Matlashov ME, Gorokhovatsky AY, Schultz C, Enikolopov G, Belousov VV. Genetically encoded fluorescent indicator for imaging NAD+/NADH ratio changes in different cellular compartments. Biochim Biophys Acta BBA-Gen Subj. 2014; 1840:951–957.10.1016/j.bbagen.2013.11.018

Borghuis BG, Marvin JS, Looger LL, Demb JB. Two-Photon Imaging of Nonlinear Glutamate Release Dynamics at Bipolar Cell Synapses in the Mouse Retina. J Neurosci. 2013; 33:10972–10985.10.1523/JNEUROSCI.1241-13.2013 [PubMed: 23825403]

Boustany NN, Boppart SA, Backman V. Microscopic imaging and spectroscopy with scattered light. Annu Rev Biomed Eng. 2010; 12:285–314.10.1146/annurev-bioeng-061008-124811 [PubMed: 20617940]

Bouwens A, Szlag D, Szkulmowski M, Bolmont T, Wojtkowski M, Lasser T. Quantitative lateral and axial flow imaging with optical coherence microscopy and tomography. Opt Express. 2013; 21:17711–17729.10.1364/OE.21.017711 [PubMed: 23938644]

Bowley, HJ.; Gerrard, DL.; Louden, JD.; Turrell, G. Practical Raman Spectroscopy, Softcover reprint of the original 1st ed. 1989. Springer; Berlin u.a: 1989.

Cai D, Cohen KB, Luo T, Lichtman JW, Sanes JR. Improved tools for the Brainbow toolbox. Nat Methods. 2013; 10:540–547.10.1038/nmeth.2450

Camp CH Jr, Lee YJ, Heddleston JM, Hartshorn CM, Walker ARH, Rich JN, Lathia JD, Cicerone MT. High-speed coherent Raman fingerprint imaging of biological tissues. Nat Photonics. 2014; 8:627–634.10.1038/nphoton.2014.145 [PubMed: 25621002]

Canty AJ, Huang L, Jackson JS, Little GE, Knott G, Maco B, De Paola V. In-vivo single neuron axotomy triggers axon regeneration to restore synaptic density in specific cortical circuits. Nat Commun. 2013; 410.1038/ncomms3038

Carter RE, Aiba I, Dietz RM, Sheline CT, Shuttleworth CW. Spreading depression and related events are significant sources of neuronal Zn2+ release and accumulation. J Cereb Blood Flow Metab Off J Int Soc Cereb Blood Flow Metab. 2011; 31:1073–1084.10.1038/jcbfm.2010.183

Chalfie M, Tu Y, Euskirchen G, Ward WW, Prasher DC. Green fluorescent protein as a marker for gene expression. Science. 1994; 263:802–805. [PubMed: 8303295]

Cheng MY, Wang EH, Woodson WJ, Wang S, Sun G, Lee AG, Arac A, Fenno LE, Deisseroth K, Steinberg GK. Optogenetic neuronal stimulation promotes functional recovery after stroke. Proc Natl Acad Sci. 2014; 111:12913–12918.10.1073/pnas.l404109111 [PubMed: 25136109]

Chen TW, Wardill TJ, Sun Y, Pulver SR, Renninger SL, Baohan A, Schreiter ER, Kerr RA, Orger MB, Jayaraman V, Looger LL, Svoboda K, Kim DS. Ultrasensitive fluorescent proteins for imaging neuronal activity. Nature. 2013; 499:295–300.10.1038/naturel2354 [PubMed: 23868258]

Chong SP, Merkle CW, Leahy C, Radhakrishnan H, Srinivasan VJ. Quantitative microvascular hemoglobin mapping using visible light spectroscopic Optical Coherence Tomography. Biomed Opt Express. 2015; 6:1429–1450.10.1364/BOE.6.001429 [PubMed: 25909026]

Chudakov DM, Matz MV, Lukyanov S, Lukyanov KA. Fluorescent Proteins and Their Applications in Imaging Living Cells and Tissues. Physiol Rev. 2010; 90:1103–1163.10.1152/physrev.00038.2009 [PubMed: 20664080]

Chuquet J, Quilichini P, Nimchinsky EA, Buzsáki G. Predominant Enhancement of Glucose Uptake in Astrocytes versus Neurons during Activation of the Somatosensory Cortex. J Neurosci. 2010; 30:15298–15303.10.1523/JNEUROSCI.0762-10.2010 [PubMed: 21068334]

Cianchetti FA, Kim DH, Dimiduk S, Nishimura N, Schaffer CB. Stimulus-evoked calcium transients in somatosensory cortex are temporarily inhibited by a nearby microhemorrhage. PloS One. 2013; 8:e65663.10.1371/journal.pone.0065663 [PubMed: 23724147]

Davalos D, Grutzendler J, Yang G, Kim JV, Zuo Y, Jung S, Littman DR, Dustin ML, Gan WB. ATP mediates rapid microglial response to local brain injury in vivo. Nat Neurosci. 2005; 8:752–758.10.1038/nnl472 [PubMed: 15895084]

Dean KM, Qin Y, Palmer AE. Visualizing metal ions in cells: An overview of analytical techniques, approaches, and probes. Biochim Biophys Acta BBA - Mol Cell Res, Cell Biology of Metals. 2012; 1823:1406–1415.10.1016/j.bbamcr.2012.04.001

Deliolanis NC, Ale A, Morscher S, Burton NC, Schaefer K, Radrich K, Razansky D, Ntziachristos V. Deep-Tissue Reporter-Gene Imaging with Fluorescence and Optoacoustic Tomography: A Performance Overview. Mol Imaging Biol. 2014; 16:652–660.10.1007/s11307-014-0728-l [PubMed: 24609633]

Denk W, Strickler JH, Webb WW. Two-photon laser scanning fluorescence microscopy. Science. 1990; 248:73–76.10.1126/science.2321027 [PubMed: 2321027]

Devor A, Sakadžić S, Saisan PA, Yaseen MA, Roussakis E, Srinivasan VJ, Vinogradov SA, Rosen BR, Buxton RB, Dale AM, Boas DA. “Overshoot” of O2 Is Required to Maintain Baseline Tissue Oxygenation at Locations Distal to Blood Vessels. J Neurosci. 2011; 31:13676–13681.10.1523/JNEUROSCI.1968-11.2011 [PubMed: 21940458]

Dong X, Heo CH, Chen S, Kim HM, Liu Z. Quinoline-Based Two-Photon Fluorescent Probe for Nitric Oxide in Live Cells and Tissues. Anal Chem. 2013; 86:308–311.10.1021/ac403226h [PubMed: 24341482]

Drew PJ, Shih AY, Driscoll JD, Knutsen PM, Blinder P, Davalos D, Akassoglou K, Tsai PS, Kleinfeld D. Chronic optical access through a polished and reinforced thinned skull. Nat Methods. 2010; 7:981–984.10.1038/nmeth.l530 [PubMed: 20966916]

Drexler, W.; Fujimoto, JG. Optical Coherence Tomography - Technology and Applications, Biological and Medical Physics, Biomedical Engineering. Springer; Berlin Heidelberg: 2008.

Driscoll JD, Shih AY, Iyengar S, Field JJ, White GA, Squier JA, Cauwenberghs G, Kleinfeld D. Photon counting, censor corrections, and lifetime imaging for improved detection in two-photon microscopy. J Neurophysiol. 2011; 105:3106–3113.10.1152/jn.00649.2010 [PubMed: 21471395]

Esipova TV, Vinogradov SA. Synthesis of Phosphorescent Asymmetrically π-Extended Porphyrins for Two-Photon Applications. J Org Chem. 2014; 79:8812–8825.10.1021/jo501521x [PubMed: 25157580]

Feng G, Mellor RH, Bernstein M, Keller-Peck C, Nguyen QT, Wallace M, Nerbonne JM, Lichtman JW, Sanes JR. Imaging Neuronal Subsets in Transgenic Mice Expressing Multiple Spectral Variants of GFP. Neuron. 2000; 28:41–51.10.1016/S0896-6273(00)00084-2 [PubMed: 11086982]

Finikova OS, Lebedev AY, Aprelev A, Troxler T, Gao F, Garnacho C, Muro S, Hochstrasser RM, Vinogradov SA. Oxygen Microscopy by Two-Photon-Excited Phosphorescence. ChemPhysChem. 2008; 9:1673–1679.10.1002/cphc.200800296 [PubMed: 18663708]

Fish, KN. Total Internal Reflection Fluorescence (TIRF) Microscopy, in: Current Protocols in Cytometry. John Wiley & Sons, Inc; 2001.

Foerch C, Rosidi NL, Schlunk F, Lauer A, Cianchetti FA, Mandeville E, Arai K, Yigitkanli K, Fan X, Wang X, van Leyen K, Steinmetz H, Schaffer CB, Lo EH. Intravenous tPA Therapy Does Not Worsen Acute Intracerebral Hemorrhage in Mice. PLoS ONE. 2013; 8:e54203.10.1371/journal.pone.0054203 [PubMed: 23408937]

Giepmans BNG, Adams SR, Ellisman MH, Tsien RY. The fluorescent toolbox for assessing protein location and function. Science. 2006; 312:217–224.10.1126/science.1124618 [PubMed: 16614209]

Grienberger C, Konnerth A. Imaging Calcium in Neurons. Neuron. 2012; 73:862–885.10.1016/j.neuron.2012.02.011 [PubMed: 22405199]

Grynkiewicz G, Poenie M, Tsien RY. A new generation of Ca2+ indicators with greatly improved fluorescence properties. J Biol Chem. 1985; 260:3440–3450. [PubMed: 3838314]

Guo H, Aleyasin H, Dickinson BC, Haskew-Layton RE, Ratan RR. Recent advances in hydrogen peroxide imaging for biological applications. Cell Biosci. 2014; 4:64.10.1186/2045-3701-4-64 [PubMed: 25400906]

Guo Z, Kim GH, Shin I, Yoon J. A cyanine-based fluorescent sensor for detecting endogenous zinc ions in live cells and organisms. Biomaterials. 2012; 33:7818–7827.10.1016/j.biomaterials.2012.07.014 [PubMed: 22871424]

Gutscher M, Pauleau AL, Marty L, Brach T, Wabnitz GH, Samstag Y, Meyer AJ, Dick TP. Real-time imaging of the intracellular glutathione redox potential. Nat Methods. 2008; 5:553–559.10.1038/nmeth.l212 [PubMed: 18469822]

Hall CN, Reynell C, Gesslein B, Hamilton NB, Mishra A, Sutherland BA, O'Farrell FM, Buchan AM, Lauritzen M, Attwell D. Capillary pericytes regulate cerebral blood flow in health and disease. Nature. 2014; 508:55–60.10.1038/naturel3165 [PubMed: 24670647]

Han J, Burgess K. Fluorescent indicators for intracellular pH. Chem Rev. 2010; 110:2709–2728.10.1021/cr900249z [PubMed: 19831417]

Harbig K, Chance B, Kovach AG, Reivich M. In vivo measurement of pyridine nucleotide fluorescence from cat brain cortex. J Appl Physiol. 1976; 41:480–488. [PubMed: 186025]

Hartmann DA, Underly RG, Watson AN, Shin AY. A murine toolbox for imaging the neurovascular unit. Microcirculation n/a–n/a. 201410.1111/micc.l2176

Heikal AA. Intracellular coenzymes as natural biomarkers for metabolic activities and mitochondrial anomalies. Biomark Med. 2010; 4:241–263.10.2217/bmm.l0.1 [PubMed: 20406068]

Helmchen F, Denk W. Deep tissue two-photon microscopy. Nat Methods. 2005; 2:932–940.10.1038/nmeth818 [PubMed: 16299478]

Hill RA, Grutzendler J. In vivo imaging of oligodendrocytes with sulforhodamine 101. Nat Methods. 2014; 11:1081–1082.10.1038/nmeth.3140 [PubMed: 25357236]

Hoover EE, Squier JA. Advances in multiphoton microscopy technology. Nat Photonics. 2013; 7:93–101.10.1038/nphoton.2012.361 [PubMed: 24307915]

Horton NG, Wang K, Kobat D, Clark CG, Wise FW, Schaffer CB, Xu C. In vivo three-photon microscopy of subcortical structures within an intact mouse brain. Nat Photonics. 2013; 7:205–209.10.1038/nphoton.2012.336

Huang B, Jones SA, Brandenburg B, Zhuang X. Whole-cell 3D STORM reveals interactions between cellular structures with nanometer-scale resolution. Nat Methods. 2008; 5:1047–1052.10.1038/nmeth.l274 [PubMed: 19029906]

Huang S, Heikal AA, Webb WW. Two-photon fluorescence spectroscopy and microscopy of NAD(P)H and flavoprotein. Biophys J. 2002; 82:2811–2825.10.1016/S0006-3495(02)75621-X [PubMed: 11964266]

Hughes EG, Kang SH, Fukaya M, Bergles DE. Oligodendrocyte progenitors balance growth with self-repulsion to achieve homeostasis in the adult brain. Nat Neurosci. 2013; 16:668–676.10.1038/nn.3390 [PubMed: 23624515]

Hung YP, Albeck JG, Tantama M, Yellen G. Imaging cytosolic NADH-NAD(+) redox state with a genetically encoded fluorescent biosensor. Cell Metab. 2011; 14:545–554.10.1016/j.cmet.2011.08.012 [PubMed: 21982714]

Hung, YP.; Yellen, G. Live-Cell Imaging of Cytosolic NADH–NAD+ Redox State Using a Genetically Encoded Fluorescent Biosensor. In: Zhang, J.; Ni, Q.; Newman, RH., editors. Fluorescent Protein-Based Biosensors, Methods in Molecular Biology. Humana Press; 2014. p. 83-95.

Hu, S.; Gonzales, E.; Soetikno, B.; Gong, E.; Yan, P.; Maslov, K.; Lee, JM.; Wang, LV. Optical-resolution photoacoustic microscopy of ischemic stroke. Photons Plus Ultrasound: Imaging and Sensing 2011, Proc SPIE7899; Presented at the Photonics West; San Francisco, California, USA. 2011. p. 789906-5.789906

Hu S, Maslov K, Tsytsarev V, Wang LV. Functional transcranial brain imaging by optical-resolution photoacoustic microscopy. J Biomed Opt. 2009; 14:040503–3. 040503. 10.1117/1.3194136 [PubMed: 19725708]

Iliff JJ, Chen MJ, Plog BA, Zeppenfeld DM, Soltero M, Yang L, Singh I, Deane R, Nedergaard M. Impairment of Glymphatic Pathway Function Promotes Tau Pathology after Traumatic Brain Injury. J Neurosci. 2014; 34:16180–16193.10.1523/JNEUROSCI.3020-14.2014 [PubMed: 25471560]

Iliff JJ, Wang M, Zeppenfeld DM, Venkataraman A, Plog BA, Liao Y, Deane R, Nedergaard M. Cerebral Arterial Pulsation Drives Paravascular CSF–Interstitial Fluid Exchange in the Murine Brain. J Neurosci. 2013; 33:18190–18199.10.1523/JNEUROSCI.1592-13.2013 [PubMed: 24227727]

Imamura H, Nhat KPH, Togawa H, Saito K, Iino R, Kato-Yamada Y, Nagai T, Noji H. Visualization of ATP levels inside single living cells with fluorescence resonance energy transfer-based genetically encoded indicators. Proc Natl Acad Sci. 2009; 106:15651–15656.10.1073/pnas.0904764106 [PubMed: 19720993]

Jia Y, Alkayed N, Wang RK. Potential of optical microangiography to monitor cerebral blood perfusion and vascular plasticity following traumatic brain injury in mice in vivo. J Biomed Opt. 2009; 14:040505–3. 040505. 10.1117/1.3207121 [PubMed: 19725710]

Kamoun WS, Chae SS, Lacorre DA, Tyrrell JA, Mitre M, Gillissen MA, Fukumura D, Jain RK, Munn LL. Simultaneous measurement of RBC velocity, flux, hematocrit and shear rate in vascular networks. Nat Methods. 2010; 7:655–660.10.1038/nmeth.l475 [PubMed: 20581828]

Kasischke KA, Lambert EM, Panepento B, Sun A, Gelbard HA, Burgess RW, Foster TH, Nedergaard M. Two-photon NADH imaging exposes boundaries of oxygen diffusion in cortical vascular supply regions. J Cereb Blood Flow Metab. 2011; 31:68–81.10.1038/jcbfm.2010.158 [PubMed: 20859293]

Kasischke KA, Vishwasrao HD, Fisher PJ, Zipfel WR, Webb WW. Neural activity triggers neuronal oxidative metabolism followed by astrocytic glycolysis. Science. 2004; 305:99–103.10.1126/science.l096485 [PubMed: 15232110]

Kazmi SMS, Salvaggio AJ, Estrada AD, Hemati MA, Shaydyuk NK, Roussakis E, Jones TA, Vinogradov SA, Dunn AK. Three-dimensional mapping of oxygen tension in cortical arterioles before and afterocclusion. Biomed Opt Express. 2013; 4:1061–1073.10.1364/BOE.4.001061 [PubMed: 23847732]

Kim HJ, Heo CH, Kim HM. Benzimidazole-Based Ratiometric Two-Photon Fluorescent Probes for Acidic pH in Live Cells and Tissues. J Am Chem Soc. 2013; 135:17969–17977.10.1021/ja409971k [PubMed: 24237203]

Kleinfeld D, Mitra PP, Helmchen F, Denk W. Fluctuations and stimulus-induced changes in blood flow observed in individual capillaries in layers 2 through 4 of rat neocortex. Proc Natl Acad Sci. 1998; 95:15741–15746.10.1073/pnas.95.26.15741 [PubMed: 9861040]

Klonoff DC. Overview of Fluorescence Glucose Sensing: A Technology with a Bright Future. J Diabetes Sci Technol. 2012; 6:1242–1250.10.1177/193229681200600602 [PubMed: 23294768]

Knowland D, Arac A, Sekiguchi KJ, Hsu M, Lutz SE, Perrino J, Steinberg GK, Barres BA, Nimmerjahn A, Agalliu D. Stepwise Recruitment of Transcellular and Paracellular Pathways Underlies Blood-Brain Barrier Breakdown in Stroke. Neuron. 2014; 82:603–617.10.1016/j.neuron.2014.03.003 [PubMed: 24746419]

Kobat D, Horton NG, Xu C. In vivo two-photon microscopy to 1.6-mm depth in mouse cortex. J Biomed Opt. 2011; 16:106014–4. 106014. 10.1117/1.3646209 [PubMed: 22029361]

Kremers GJ, Gilbert SG, Cranfill PJ, Davidson MW, Piston DW. Fluorescent proteins at a glance. J Cell Sci. 2011; 124:157–160.10.1242/jcs.072744 [PubMed: 21187342]

Kuchibhotla KV, Lattarulo CR, Hyman BT, Bacskai BJ. Synchronous hyperactivity and intercellular calcium waves in astrocytes in Alzheimer mice. Science. 2009; 323:1211–1215.10.1126/science.1169096 [PubMed: 19251629]

Lam CK, Yoo T, Hiner B, Liu Z, Grutzendler J. Embolus extravasation is an alternative mechanism for cerebral microvascular recanalization. Nature. 2010; 465:478–482.10.1038/nature09001 [PubMed: 20505729]

Lebedev AY, Cheprakov AV, Sakadžić S, Boas DA, Wilson DF, Vinogradov SA. Dendritic Phosphorescent Probes for Oxygen Imaging in Biological Systems. ACS Appl Mater Interfaces. 2009; 1:1292–1304.10.1021/am9001698 [PubMed: 20072726]

Lecoq J, Parpaleix A, Roussakis E, Ducros M, Houssen YG, Vinogradov SA, Charpak S. Simultaneous two-photon imaging of oxygen and blood flow in deep cerebral vessels. Nat Med. 2011; 17:893–898.10.1038/nm.2394 [PubMed: 21642977]

Lee HY, Lee JJ, Park J, Park SB. Development of Fluorescent Glucose Bioprobes and Their Application on Real-Time and Quantitative Monitoring of Glucose Uptake in Living Cells. Chem –Eur J. 2011; 17:143–150.10.1002/chem.201002560 [PubMed: 21207611]

Lee J, Jiang JY, Wu W, Lesage F, Boas DA. Statistical intensity variation analysis for rapid volumetric imaging of capillary network flux. Biomed Opt Express. 2014; 5:1160–1172.10.1364/BOE.5.001160 [PubMed: 24761298]

Lee J, Radhakrishnan H, Wu W, Daneshmand A, Climov M, Ayata C, Boas DA. Quantitative imaging of cerebral blood flow velocity and intracellular motility using dynamic light scattering–optical coherence tomography. J Cereb Blood Flow Metab. 2013a; 33:819–825.10.1038/jcbfm.2013.20 [PubMed: 23403378]

Lee J, Wu W, Lesage F, Boas DA. Multiple-capillary measurement of RBC speed, flux, and density with optical coherence tomography. J Cereb Blood Flow Metab. 2013b; 33:1707–1710.10.1038/jcbfm.2013.158 [PubMed: 24022621]

Liemburg-Apers DC, Imamura H, Forkink M, Nooteboom M, Swarts HG, Brock R, Smeitink JAM, Willems PHGM, Koopman WJH. Quantitative Glucose and ATP Sensing in Mammalian Cells. Pharm Res. 2011; 28:2745–2757.10.1007/s11095-011-0492-8 [PubMed: 21691894]

Li L, Maslov KI, Ku G, Wang LV. In-vivo imaging of microcirculation using integrated photoacoustic and optical-coherence microscopy. 2009:717701–8. 717701. 10.1117/12.809323

Li L, Zemp RJ, Lungu G, Stoica G, Wang LV. Photoacoustic imaging of lacZ gene expression in vivo. J Biomed Opt. 2007; 12:020504–3. 020504. 10.1117/1.2717531 [PubMed: 17477703]

Li P, Murphy TH. Two-Photon Imaging during Prolonged Middle Cerebral Artery Occlusion in Mice Reveals Recovery of Dendritic Structure after Reperfusion. J Neurosci. 2008; 28:11970–11979.10.1523/JNEUROSCI.3724-08.2008 [PubMed: 19005062]

Liu X, Huang Y, Ramella-Roman JC, Mathews SA, Kang JU. Quantitative transverse flow measurement using optical coherence tomography speckle decorrelation analysis. Opt Lett. 2013; 38:805–807.10.1364/OL.38.000805 [PubMed: 23455305]

Lu CD, Kraus MF, Potsaid B, Liu JJ, Choi W, Jayaraman V, Cable AE, Hornegger J, Duker JS, Fujimoto JG. Handheld ultrahigh speed swept source optical coherence tomography instrument

using a MEMS scanning mirror. Biomed Opt Express. 2014; 5:293–311.10.1364/BOE.5.000293 [PubMed: 24466495]

Marvin JS, Borghuis BG, Tian L, Cichon J, Harnett MT, Akerboom J, Gordus A, Renninger SL, Chen TW, Bargmann CI, Orger MB, Schreiter ER, Demb JB, Gan WB, Hires SA, Looger LL. An optimized fluorescent probe for visualizing glutamate neurotransmission. Nat Methods. 2013; 10:162–170.10.1038/nmeth.2333 [PubMed: 23314171]

Mascaro ALA, Cesare P, Sacconi L, Grasselli G, Mandolesi G, Maco B, Knott GW, Huang L, Paola VD, Strata P, Pavone FS. In vivo single branch axotomy induces GAP-43–dependent sprouting and synaptic remodeling in cerebellar cortex. Proc Natl Acad Sci. 2013; 110:10824–10829.10.1073/pnas.l219256110 [PubMed: 23754371]

Maslov K, Zhang HF, Hu S, Wang LV. Optical-resolution photoacoustic microscopy for in vivo imaging of single capillaries. Opt Lett. 2008; 33:929–931.10.1364/OL33.000929 [PubMed: 18451942]

Matthews TP, Zhang C, Yao DK, Maslov K, Wang LV. Label-free photoacoustic microscopy of peripheral nerves. J Biomed Opt. 2014; 19:016004–016004.10.1117/l.JBO.19.1.016004

Michalski D, Grosche J, Pelz J, Schneider D, Weise C, Bauer U, Kacza J, Gärtner U, Hobohm C, Härtig W. A novel quantification of blood–brain barrier damage and histochemical typing after embolic stroke in rats. Brain Res. 2010; 1359:186–200.10.1016/j.brainres.2010.08.045 [PubMed: 20732314]

Milesi S, Boussadia B, Plaud C, Catteau M, Rousset MC, De Bock F, Schaeffer M, Lerner-Natoli M, Rigau V, Marchi N. Redistribution of PDGFRβ cells and NG2DsRed pericytes at the cerebrovasculature after status epilepticus. Neurobiol Dis. 2014; 71:151–158.10.1016/j.nbd.2014.07.010 [PubMed: 25088711]

Milner, R. Astrocytes - Methods and Protocols, Methods in Molecular Biology. Humana Press; 2012.

Nägerl UV, Willig KI, Hein B, Hell SW, Bonhoeffer T. Live-cell imaging of dendritic spines by STED microscopy. Proc Natl Acad Sci. 2008; 105:18982–18987.10.1073/pnas.0810028105 [PubMed: 19028874]

Niklass S, Stoyanov S, Garz C, Bueche CZ, Mencl S, Reymann K, Heinze HJ, Carare RO, Kleinschnitz C, Schreiber S. Intravital imaging in spontaneously hypertensive stroke-prone rats-a pilot study. Exp Transl Stroke Med. 2014; 6:1.10.1186/2040-7378-6-l [PubMed: 24461046]

Nimmerjahn A, Kirchhoff F, Helmchen F. Resting microglial cells are highly dynamic surveillants of brain parenchyma in vivo. Science. 2005; 308:1314–1318.10.1126/science.1110647 [PubMed: 15831717]

Nimmerjahn A, Kirchhoff F, Kerr JND, Helmchen F. Sulforhodamine 101 as a specific marker of astroglia in the neocortex in vivo. Nat Methods. 2004; 1:31–37.10.1038/nmeth706 [PubMed: 15782150]

Nishimura N, Rosidi NL, ladecola C, Schaffer CB. Limitations of collateral flow after occlusion of a single cortical penetrating arteriole. J Cereb Blood Flow Metab. 2010; 30:1914–1927.10.1038/jcbfm.2010.157 [PubMed: 20842163]

Nishimura N, Schaffer CB, Friedman B, Lyden PD, Kleinfeld D. Penetrating arterioles are a bottleneck in the perfusion of neocortex. Proc Natl Acad Sci. 2007; 104:365–370.10.1073/pnas.0609551104 [PubMed: 17190804]

Nishimura N, Schaffer CB, Friedman B, Tsai PS, Lyden PD, Kleinfeld D. Targeted insult to subsurface cortical blood vessels using ultrashort laser pulses: three models of stroke. Nat Methods. 2006; 3:99–108.10.1038/nmeth844 [PubMed: 16432519]

Nishiyama A, Komitova M, Suzuki R, Zhu X. Polydendrocytes (NG2 cells): multifunctional cells with lineage plasticity. Nat Rev Neurosci. 2009; 10:9–22.10.1038/nrn2495 [PubMed: 19096367]

Noguchi J, Nagaoka A, Watanabe S, Ellis-Davies GCR, Kitamura K, Kano M, Matsuzaki M, Kasai H. In vivo two-photon uncaging of glutamate revealing the structure-function relationships of dendritic spines in the neocortex of adult mice. J Physiol. 2011; 589:2447–2457.10.1113/jphysiol.2011.207100 [PubMed: 21486811]

O'Hare HM, Johnsson K, Gautier A. Chemical probes shed light on protein function. Curr Opin Struct Biol, Membranes/Engineering and design. 2007; 17:488–494.10.1016/j.sbi.2007.07.005

Okumoto S, Looger LL, Micheva KD, Reimer RJ, Smith SJ, Frommer WB. Detection of glutamate release from neurons by genetically encoded surface-displayed FRET nanosensors. Proc Natl Acad Sci U S A. 2005; 102:8740–8745.10.1073/pnas.0503274102 [PubMed: 15939876]

Padmawar P, Yao X, Bloch O, Manley GT, Verkman AS. K+ waves in brain cortex visualized using a long-wavelength K+-sensing fluorescent indicator. Nat Methods. 2005; 2:825–827.10.1038/nmeth801 [PubMed: 16278651]

Parpaleix A, Houssen YG, Charpak S. Imaging local neuronal activity by monitoring P02 transients in capillaries. Nat Med. 2013; 19:241–246.10.1038/nm.3059 [PubMed: 23314058]

Penner-Hahn, JE. Technologies for Detecting Metals in Single Cells. In: Banci, L., editor. Metallomics and the Cell, Metal Ions in Life Sciences. Springer; Netherlands: 2013. p. 15-40.

Pickup JC, Hussain F, Evans ND, Rolinski OJ, Birch DJS. Fluorescence-based glucose sensors. Biosens Bioelectron, 20th Anniversary of Biosensors and Bioelectronics 20th Anniversary of Biosensors and Bioelectronics. 2005; 20:2555–2565.10.1016/j.bios.2004.10.002

Pickup JC, Khan F, Zhi ZL, Coulter J, Birch DJS. Fluorescence intensity- and lifetime-based glucose sensing using glucose/galactose-binding protein. J Diabetes Sci Technol. 2013; 7:62–71. [PubMed: 23439161]

Radford RJ, Chyan W, Lippard SJ. Peptide-based Targeting of Fluorescent Zinc Sensors to the Plasma Membrane of Live Cells. Chem Sci R Soc Chem. 2013; 20104:3080–3084.10.1039/C3SC50974E

Ren H, Du C, Yuan Z, Park K, Volkow ND, Pan Y. Cocaine-induced cortical microischemia in the rodent brain: clinical implications. Mol Psychiatry. 2012; 17:1017–1025.10.1038/mp.2011.160 [PubMed: 22124273]

Robles FE, Wilson C, Grant G, Wax A. Molecular imaging true-colour spectroscopic optical coherence tomography. Nat Photonics. 2011; 5:744–747.10.1038/nphoton.2011.257 [PubMed: 23144652]

Roussakis E, Spencer JA, Lin CP, Vinogradov SA. Two-Photon Antenna-Core Oxygen Probe with Enhanced Performance. Anal Chem. 2014; 86:5937–5945.10.1021/ac501028m [PubMed: 24848643]

Rumsey WL, Vanderkooi JM, Wilson DF. Imaging of phosphorescence: a novel method for measuring oxygen distribution in perfused tissue. Science. 1988; 241:1649–1651. [PubMed: 3420417]

Saar BG, Freudiger CW, Xu X, Huttner A, Kesari S, Young G, Xie XS. Coherent Raman tissue imaging in the brain. Cold Spring Harb Protoc. 2014 2014. 10.1101/pdb.top081695

Sakadžić S, Mandeville ET, Gagnon L, Musacchia JJ, Yaseen MA, Yucel MA, Lefebvre J, Lesage F, Dale AM, Eikermann-Haerter K, Ayata C, Srinivasan VJ, Lo EH, Devor A, Boas DA. Large arteriolar component of oxygen delivery implies a safe margin of oxygen supply to cerebral tissue. Nat Commun. 2014; 510.1038/ncomms6734

Sakadžić S, Roussakis E, Yaseen MA, Mandeville ET, Srinivasan VJ, Arai K, Ruvinskaya S, Devor A, Lo EH, Vinogradov SA, Boas DA. Two-photon high-resolution measurement of partial pressure of oxygen in cerebral vasculature and tissue. Nat Methods. 2010; 7:755–759.10.1038/nmeth.l490 [PubMed: 20693997]

San Martín A, Ceballo S, Baeza-Lehnert F, Lerchundi R, Valdebenito R, Contreras-Baeza Y, Alegría K, Barros LF. Imaging Mitochondrial Flux in Single Cells with a FRET Sensor for Pyruvate. PLoS ONE. 2014a; 9:e85780.10.1371/journal.pone.0085780 [PubMed: 24465702]

San Martín A, Ceballo S, Ruminot I, Lerchundi R, Frommer WB, Barros LF. A Genetically Encoded FRET Lactate Sensor and Its Use To Detect the Warburg Effect in Single Cancer Cells. PLoS ONE. 2013; 8:e57712.10.1371/journal.pone.0057712 [PubMed: 23469056]

San Martín A, Sotelo-Hitschfeld T, Lerchundi R, Fernández-Moncada I, Ceballo S, Valdebenito R, Baeza-Lehnert F, Alegría K, Contreras-Baeza Y, Garrido-Gerter P, Romero-Gómez I, Barros LF. Single-cell imaging tools for brain energy metabolism: a review. Neurophotonics. 2014b; 1:011004–011004.10.1117/l.NPh.l.l.011004 [PubMed: 26157964]

Sawinski J, Wallace DJ, Greenberg DS, Grossmann S, Denk W, Kerr JND. Visually evoked activity in cortical cells imaged in freely moving animals. Proc Natl Acad Sci. 2009; 106:19557–19562.10.1073/pnas.0903680106 [PubMed: 19889973]

Schaffer CB, Friedman B, Nishimura N, Schroeder LF, Tsai PS, Ebner FF, Lyden PD, Kleinfeld D. Two-Photon Imaging of Cortical Surface Microvessels Reveals a Robust Redistribution in Blood Flow after Vascular Occlusion. PLoS Biol. 2006; 4:e22.10.1371/journal.pbio.0040022 [PubMed: 16379497]

Schreiner, A.; Rose, C. Current Microscopy Contributions to Advances in Science and Technology. Formatex Research Centre; Badajoz, Spain: 2013. Quantitative imaging of intracellular sodium.

Shcherbakova DM, Verkhusha VV. Near-infrared fluorescent proteins for multicolor in vivo imaging. Nat Methods. 2013; 10:751–754.10.1038/nmeth.2521 [PubMed: 23770755]

Shen HY, Sun H, Hanthorn MM, Zhi Z, Lan JQ, Poulsen DJ, Wang RK, Boison D. Overexpression of adenosine kinase in cortical astrocytes and focal neocortical epilepsy in mice. J Neurosurg. 2014; 120:628–638.10.3171/2013.10.JNS13918 [PubMed: 24266544]

Shih AY, Driscoll JD, Drew PJ, Nishimura N, Schaffer CB, Kleinfeld D. Two-photon microscopy as a tool to study blood flow and neurovascular coupling in the rodent brain. J Cereb Blood Flow Metab. 2012; 32:1277–1309.10.1038/jcbfm.2011.196 [PubMed: 22293983]

Shroff, H.; White, H.; Betzig, E. Current Protocols in Cell Biology. John Wiley & Sons, Inc; 2001. Photoactivated Localization Microscopy (PALM) of Adhesion Complexes.

Shuttleworth CW. Use of NAD(P)H and flavoprotein autofluorescence transients to probe neuron and astrocyte responses to synaptic activation. Neurochem Int. 2010; 56:379–386.10.1016/j.neuint.2009.12.015 [PubMed: 20036704]

Sigler A, Murphy TH. In Vivo 2-Photon Imaging of Fine Structure in the Rodent Brain Before, During, and After. Stroke. 2010; 41:S117–S123.10.1161/STROKEAHA.110.594648 [PubMed: 20876484]

Simpson IA, Carruthers A, Vannucci SJ. Supply and demand in cerebral energy metabolism: the role of nutrient transporters. J Cereb Blood Flow Metab. 2007; 27:1766–1791.10.1038/sj.jcbfm.9600521 [PubMed: 17579656]

Song D, Cho S, Han Y, You Y, Nam W. Ratiometric Fluorescent Probes for Detection of Intracellular Singlet Oxygen. Org Lett. 2013; 15:3582–3585.10.1021/ol401421r [PubMed: 23808624]

Spencer JA, Ferraro F, Roussakis E, Klein A, Wu J, Runnels JM, Zaher W, Mortensen LJ, Alt C, Turcotte R, Yusuf R, Côté D, Vinogradov SA, Scadden DT, Lin CP. Direct measurement of local oxygen concentration in the bone marrow of live animals. Nature. 2014; 508:269–273.10.1038/naturel3034 [PubMed: 24590072]

Srinivasan VJ, Atochin DN, Radhakrishnan H, Jiang JY, Ruvinskaya S, Wu W, Barry S, Cable AE, Ayata C, Huang PL, Boas DA. Optical coherence tomography for the quantitative study of cerebrovascular physiology. J Cereb Blood Flow Metab. 2011; 31:1339–1345.10.1038/jcbfm.2011.19 [PubMed: 21364599]

Srinivasan VJ, Jiang JY, Yaseen MA, Radhakrishnan H, Wu W, Barry S, Cable AE, Boas DA. Rapid volumetric angiography of cortical microvasculature with optical coherence tomography. Opt Lett. 2010a; 35:43–45.10.1364/OL.35.000043 [PubMed: 20664667]

Srinivasan VJ, Mandeville ET, Can A, Blasi F, Climov M, Daneshmand A, Lee JH, Yu E, Radhakrishnan H, Lo EH, Sakadžić S, Eikermann-Haerter K, Ayata C. Multiparametric, Longitudinal Optical Coherence Tomography Imaging Reveals Acute Injury and Chronic Recovery in Experimental Ischemic Stroke. PLoS ONE. 2013; 8:e71478.10.1371/journal.pone.0071478 [PubMed: 23940761]

Srinivasan VJ, Radhakrishnan H, Jiang JY, Barry S, Cable AE. Optical coherence microscopy for deep tissue imaging of the cerebral cortex with intrinsic contrast. Opt Express. 2012a; 20:2220–2239.10.1364/OE.20.002220 [PubMed: 22330462]

Srinivasan VJ, Radhakrishnan H, Lo EH, Mandeville ET, Jiang JY, Barry S, Cable AE. OCT methods for capillary velocimetry. Biomed Opt Express. 2012b; 3:612–629.10.1364/BOE.3.000612 [PubMed: 22435106]

Srinivasan VJ, Sakadzić S, Gorczynska I, Ruvinskaya S, Wu W, Fujimoto JG, Boas DA. Quantitative cerebral blood flow with Optical Coherence Tomography. Opt Express. 2010b; 18:2477–2494.10.1364/OE.18.002477 [PubMed: 20174075]

Srinivasan VJ, Sakadzić S, Gorczynska I, Ruvinskaya S, Wu W, Fujimoto JG, Boas DA. Depth-resolved microscopy of cortical hemodynamics with optical coherence tomography. Opt Lett. 2009; 34:3086–3088.10.1364/OL.34.003086 [PubMed: 19838234]

Svoboda K, Denk W, Kleinfeld D, Tank DW. In vivo dendritic calcium dynamics in neocortical pyramidal neurons. Nature. 1997; 385:161–165.10.1038/385161a0 [PubMed: 8990119]

Svoboda K, Yasuda R. Principles of Two-Photon Excitation Microscopy and Its Applications to Neuroscience. Neuron. 2006; 50:823–839.10.1016/j.neuron.2006.05.019 [PubMed: 16772166]

Sword J, Masuda T, Croom D, Kirov SA. Evolution of neuronal and astroglial disruption in the peri-contusional cortex of mice revealed by in vivo two-photon imaging. Brain awt026. 201310.1093/brain/awt026

Takano T, Tian GF, Peng W, Lou N, Lovatt D, Hansen AJ, Kasischke KA, Nedergaard M. Cortical spreading depression causes and coincides with tissue hypoxia. Nat Neurosci. 2007; 10:754–762.10.1038/nnl902 [PubMed: 17468748]

Tantama M, Martínez-François JR, Mongeon R, Yellen G. Imaging energy status in live cells with a fluorescent biosensor of the intracellular ATP-to-ADP ratio. Nat Commun. 2013; 410.1038/ncomms3550

Thrane VR, Thrane AS, Plog BA, Thiyagarajan M, Iliff JJ, Deane R, Nagelhus EA, Nedergaard M. Paravascular microcirculation facilitates rapid lipid transport and astrocyte signaling in the brain. Sci Rep. 2013; 310.1038/srep02582

Tokayer J, Jia Y, Dhalla AH, Huang D. Blood flow velocity quantification using split-spectrum amplitude-decorrelation angiography with optical coherence tomography. Biomed Opt Express. 2013; 4:1909–1924.10.1364/BOE.4.001909 [PubMed: 24156053]

Tsytsarev V, Rao B, Maslov KI, Li L, Wang LV. Photoacoustic and optical coherence tomography of epilepsy with high temporal and spatial resolution and dual optical contrasts. J Neurosci Methods. 2013; 216:142–145.10.1016/j.jneumeth.2013.04.001 [PubMed: 23603664]

Tu H, Boppart SA. Coherent anti-Stokes Raman scattering microscopy: overcoming technical barriers for clinical translation. J Biophotonics. 2014; 7:9–22.10.1002/jbio.201300031 [PubMed: 23674234]

Turner DA, Foster KA, Galeffi F, Somjen GG. Differences in 02 availability resolve the apparent discrepancies in metabolic intrinsic optical signals in vivo and in vitro. Trends Neurosci. 2007; 30:390–398.10.1016/j.tins.2007.06.001 [PubMed: 17590447]

Vandenbroucke RE, Libert C. Is there new hope for therapeutic matrix metalloproteinase inhibition? Nat Rev Drug Discov. 2014; 13:904–927.10.1038/nrd4390 [PubMed: 25376097]

Vanderkooi JM, Maniara G, Green TJ, Wilson DF. An optical method for measurement of dioxygen concentration based upon quenching of phosphorescence. J Biol Chem. 1987; 262:5476–5482. [PubMed: 3571219]

Vishwasrao HD, Heikal AA, Kasischke KA, Webb WW. Conformational Dependence of Intracellular NADH on Metabolic State Revealed by Associated Fluorescence Anisotropy. J Biol Chem. 2005; 280:25119–25126.10.1074/jbc.M502475200 [PubMed: 15863500]

Wang D, Hurst TK, Thompson RB, Fierke CA. Genetically encoded ratiometric biosensors to measure intracellular exchangeable zinc in Escherichia coli. J Biomed Opt. 2011; 16:087011.10.1117/1.3613926 [PubMed: 21895338]

Wang L, Maslov K, Wang LV. Single-cell label-free photoacoustic flowoxigraphy in vivo. Proc Natl Acad Sci. 2013a; 110:5759–5764.10.1073/pnas.l215578110 [PubMed: 23536296]

Wang LV, Gao L. Photoacoustic Microscopy and Computed Tomography: From Bench to Bedside. Annu Rev Biomed Eng. 2014; 16:155–185.10.1146/annurev-bioeng-071813-104553 [PubMed: 24905877]

Wang LV, Hu S. Photoacoustic tomography: in vivo imaging from organelles to organs. Science. 2012; 335:1458–1462.10.1126/science.l216210 [PubMed: 22442475]

Wang L, Xia J, Yao J, Maslov K, Wang L. Ultrasonically Encoded Photoacoustic Flowgraphy in Biological Tissue. Phys Rev Lett. 2013b; 111:204301.10.1103/PhysRevLett.111.204301 [PubMed: 24289689]

Wang RK, An L. Doppler optical micro-angiography for volumetric imaging of vascular perfusion in vivo. Opt Express. 2009; 17:8926–8940.10.1364/OE.17.008926 [PubMed: 19466142]

Wang RK, Jacques SL, Ma Z, Hurst S, Hanson SR, Gruber A. Three dimensional optical angiography. Opt Express. 2007; 15:4083–4097.10.1364/OE.15.004083 [PubMed: 19532651]

Wang Y, Wang R. Autocorrelation optical coherence tomography for mapping transverse particle-flow velocity. Opt Lett. 2010; 35:3538–3540.10.1364/OL.35.003538 [PubMed: 21042342]

Watson BD, Dietrich WD, Busto R, Wachtel MS, Ginsberg MD. Induction of reproducible brain infarction by photochemically initiated thrombosis. Ann Neurol. 1985; 17:497–504.10.1002/ana.410170513 [PubMed: 4004172]

Weiss N, van Leeuwen TG, Kalkman J. Localized measurement of longitudinal and transverse flow velocities in colloidal suspensions using optical coherence tomography. Phys Rev E Stat Nonlin Soft Matter Phys. 2013; 88:042312. [PubMed: 24229177]

Wildanger D, Medda R, Kastrup L, Hell Sw. A compact STED microscope providing 3D nanoscale resolution. J Microsc. 2009; 236:35–43.10.1111/j.l365-2818.2009.03188.x [PubMed: 19772534]

Willig KI, Rizzoli SO, Westphal V, Jahn R, Hell SW. STED microscopy reveals that synaptotagmin remains clustered after synaptic vesicle exocytosis. Nature. 2006; 440:935–939.10.1038/nature04592 [PubMed: 16612384]

Winship IR, Murphy TH. In Vivo Calcium Imaging Reveals Functional Rewiring of Single Somatosensory Neurons after Stroke. J Neurosci. 2008; 28:6592–6606.10.1523/JNEUROSCI.0622-08.2008 [PubMed: 18579732]

Xu K, Wang L, Qiang M, Wang L, Li P, Tang B. A selective near-infrared fluorescent probe for singlet oxygen in living cells. Chem Commun. 2011; 47:7386–7388.10.1039/C1CC12473K

Xu W, Zhao X, Lv W, Yang H, Liu S, Liang H, Tu Z, Xu H, Qiao W, Zhao Q, Huang W. Rational Design of Phosphorescent Chemodosimeter for Reaction-Based One- and Two-Photon and Time-Resolved Luminescent Imaging of Biothiols in Living Cells. Adv Healthc Mater. 2014; 3:658–669.10.1002/adhm.201300278 [PubMed: 24243822]

Xu Z, Zhu Q, Wang LV. In vivo photoacoustic tomography of mouse cerebral edema induced by cold injury. J Biomed Opt. 2011; 16:066020–4. 066020. 10.1117/1.3584847 [PubMed: 21721821]

Yang C. Molecular contrast optical coherence tomography: a review. Photochem Photobiol. 2005; 81:215–237.10.1562/2004-08-06-IR-266 [PubMed: 15588122]

Yao DK, Maslov K, Shung KK, Zhou Q, Wang LV. In vivo label-free photoacoustic microscopy of cell nuclei by excitation of DNA and RNA. Opt Lett. 2010; 35:4139–4141.10.1364/OL.35.004139 [PubMed: 21165116]

Yao J, Maslov KI, Shi Y, Taber LA, Wang LV. In vivo photoacoustic imaging of transverse blood flow by using Doppler broadening of bandwidth. Opt Lett. 2010; 35:1419–1421.10.1364/OL.35.001419 [PubMed: 20436589]

Yao J, Wang LV. Photoacoustic Brain Imaging: from Microscopic to Macroscopic Scales. Neurophotonics. 2014; 110.1117/1.NPh.1.1.011003

Yao J, Xia J, Maslov KI, Nasiriavanaki M, Tsytsarev V, Demchenko AV, Wang LV. Noninvasive photoacoustic computed tomography of mouse brain metabolism in vivo. NeuroImage. 2013; 64:257–266.10.1016/j.neuroimage.2012.08.054 [PubMed: 22940116]

Yaseen MA, Sakadžić S, Wu W, Becker W, Kasischke KA, Boas DA. In vivo imaging of cerebral energy metabolism with two-photon fluorescence lifetime microscopy of NADH. Biomed Opt Express. 2013; 4:307–321.10.1364/BOE.4.000307 [PubMed: 23412419]

Yemisci M, Gursoy-Ozdemir Y, Vural A, Can A, Topalkara K, Dalkara T. Pericyte contraction induced by oxidative-nitrative stress impairs capillary reflow despite successful opening of an occluded cerebral artery. Nat Med. 2009; 15:1031–1037.10.1038/nm.2022 [PubMed: 19718040]

Yi J, Chen S, Backman V, Zhang HF. In vivo functional microangiography by visible-light optical coherence tomography. Biomed Opt Express. 2014; 5:3603–3612.10.1364/BOE.5.003603 [PubMed: 25360376]

You Y, Lee S, Kim T, Ohkubo K, Chae WS, Fukuzumi S, Jhon GJ, Nam W, Lippard SJ. Phosphorescent Sensor for Biological Mobile Zinc. J Am Chem Soc. 2011; 133:18328–18342.10.1021/ja207163r [PubMed: 22023085]

Yu H, Xiao Y, Jin L. A Lysosome-Targetable and Two-Photon Fluorescent Probe for Monitoring Endogenous and Exogenous Nitric Oxide in Living Cells. J Am Chem Soc. 2012; 134:17486–17489.10.1021/ja308967u [PubMed: 23043509]

Yuzawa I, Sakadžić S, Srinivasan VJ, Shin HK, Eikermann-Haerter K, Boas DA, Ayata C. Cortical spreading depression impairs oxygen delivery and metabolism in mice. J Cereb Blood Flow Metab. 2012; 32:376–386.10.1038/jcbfm.2011.148 [PubMed: 22008729]

Zhang C, Zhang YS, Yao DK, Xia Y, Wang LV. Label-free photoacoustic microscopy of cytochromes. J Biomed Opt. 2013; 18:020504–020504.10.1117/1.JBO.18.2.020504

Zhang, J.; Ni, Q.; Newman, RH. Fluorescent Protein-Based Biosensors - Methods and Protocols, Methods in Molecular Biology. Springer Science+Business Media; 2014.

Zhang S, Boyd J, Delaney K, Murphy TH. Rapid Reversible Changes in Dendritic Spine Structure In Vivo Gated by the Degree of Ischemia. J Neurosci. 2005; 25:5333–5338.10.1523/JNEUROSCI.1085-05.2005 [PubMed: 15930381]

Zhang S, Murphy TH. Imaging the Impact of Cortical Microcirculation on Synaptic Structure and Sensory-Evoked Hemodynamic Responses In Vivo. PLoS Biol. 2007; 5:e119.10.1371/journal.pbio.0050119 [PubMed: 17456007]

Zhao Y, Jin J, Hu Q, Zhou HM, Yi J, Yu Z, Xu L, Wang X, Yang Y, Loscalzo J. Genetically encoded fluorescent sensors for intracellular NADH detection. Cell Metab. 2011; 14:555–566.10.1016/j.cmet.2011.09.004 [PubMed: 21982715]

Zhu X, Bergles DE, Nishiyama A. NG2 cells generate both oligodendrocytes and gray matter astrocytes. Development. 2008; 135:145–157.10.1242/dev.004895 [PubMed: 18045844]

Highlights

1. Reviewing high-resolution optical technologies for *in vivo* brain imaging
2. Numerous choices exist for imaging cellular structure
3. Only few functional markers are in use
4. Probe design and imaging technology are rapidly improving

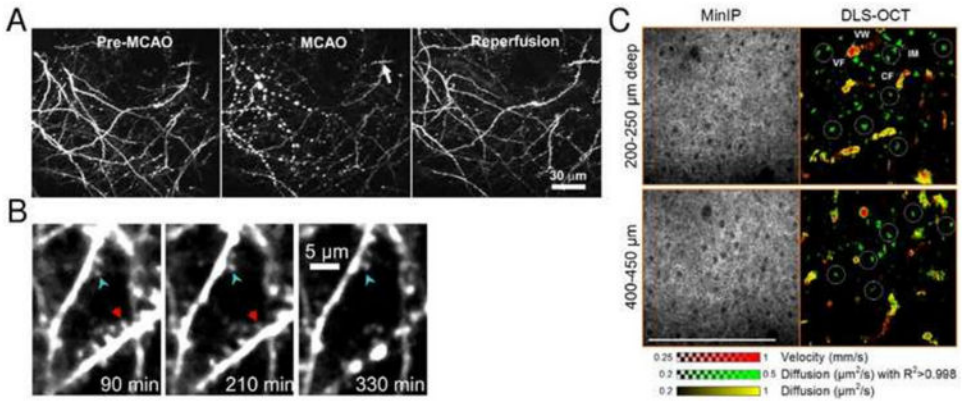

Fig. 1.

Imaging neuronal morphology. (A) Two-photon imaging of local changes in dendritic structure before, during, and after MCAO. The middle panels were taken during 52 min after MCAO shows extensive dendritic beading. Reperfusion significantly restores dendritic structure. Adapted with permission from Li and Murphy (2008). (B) Two-photon imaging of focal dendritic damage near ischemic border-zone induced by photothrombosis in mouse cortex. Arrowheads point to a stable dendrite with preserved spines (blue arrowhead) adjacent to a dendrite that developed beading (red arrowhead) 5.5 h after stroke near the border region. Adapted with permission from Zhang and Murphy (2007). (C) Label-free dynamic light scattering-optical coherence tomography (DLS-OCT) imaging of neuronal intracellular motility in rat cortex, with a high magnification objective (40×). The velocity and diffusion maps (red and yellow) are superimposed with the map of diffusion with high R2 (green). White circles show the spatial correlation between the positions of neuronal cell bodies (dark spots in minimum intensity projection, MinIP) and neuronal intracellular organelle motility (IM; green spots). Not all cell bodies are marked. BF, blood flow; and VW, vessel wall. The small range of the diffusion coefficient is used to increase the image contrast. Scale bar = 200 μm. Adapted with permission from Lee et al. (2013a).

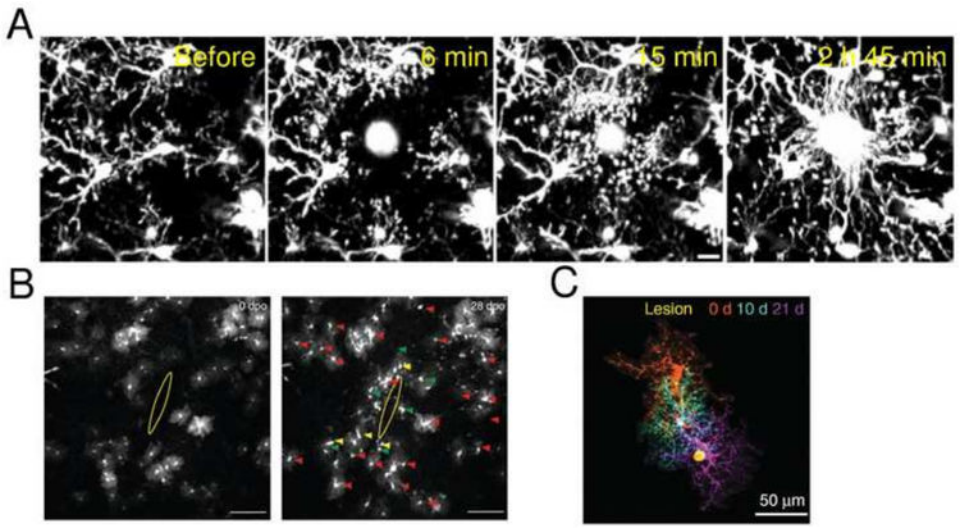

Fig. 2.

Imaging glial morphology. (A) Microglial processes move rapidly towards the site of localized injury inside the cortex induced by the ablation via femtosecond laser excitation. Imaging of GFP-expressing parenchymal microglia was performed through the thinned skull of anesthetized heterozygous C×3cr1$^{GFP/+}$ mice. Scale bar = 10 μm. Adapted with permission from Davalos et al. (2005). (B) Live imaging of astrocyte responses to a punctate lesion. GFP-labeled astrocytes (white) in the vicinity of a punctate lesion (yellow ellipse) in the somatosensory cortex of GLAST/eGFP mice, imaged *in vivo* by MPM at 0 and 28 days after injury. Imaging revealed a markedly heterogeneous reaction: the majority of astrocytes retained a stable morphology (red arrowheads), and only a few cells became polarized toward the injury site (yellow arrowheads) and/or underwent cell division (green arrowheads). Scale bars = 100 μm. Adapted with permission from Bardehle et al. (2013). (C) MPM imaging of NG2+ cells after focal laser cortical lesion in NG2-mEGFP mice. NG2+ cells surround areas of CNS damage and proliferate to maintain their density. Montage of three images of one NG2+ cell collected on different days showing the migration of the cell toward the lesion (yellow). Adapted with permission from Huges et al. (2013).

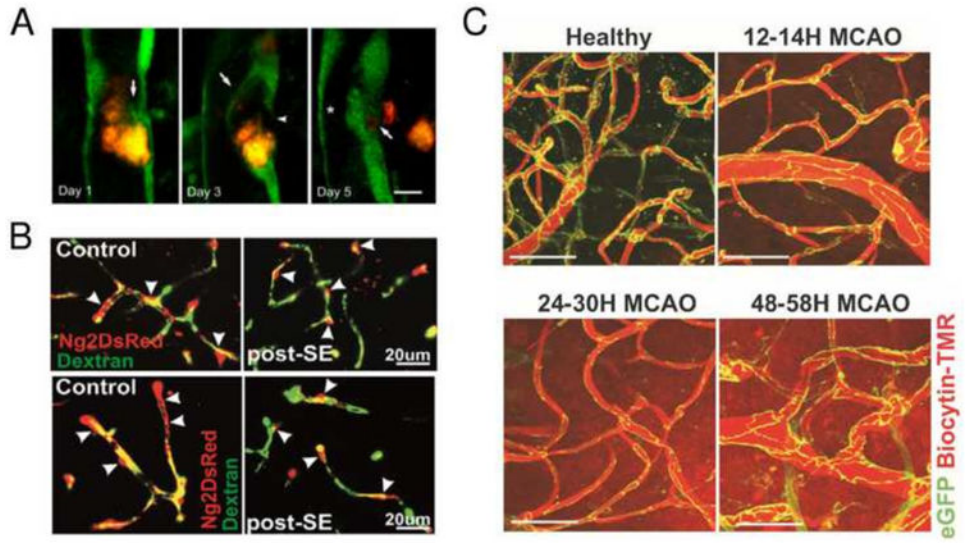

Fig. 3.

Imaging vascular morphology. (A) Focal endothelial remodeling underlies the translocation of emboli. Time-lapse MPM imaging in Tie2–GFP mice shows the gradual extension of a membrane from the adjacent endothelium (arrow, day 1) eventually surrounding a cholesterol embolus (orange) (arrow, day 3). The original endothelium undergoes retraction (arrowhead, day 3) creating a path for embolus translocation. On day 5 the embolus has extravasated, leading to lumen recanalization (asterisk). Scale bar = 10 μm. Adapted with permission from Lam et al. (2010). (B) Pattern of NG2DsRed cerebrovascular coverage after severe status epilepticus (SE) *in vivo* imaged by MPM. In control NG2DsRed transgenic mice, approximately 60–80% of the cortical microvessel surface is covered by pericytes. FITC-dextran was used to visualize the cerebrovascular tree. Following severe SE (post-SE), retraction of NG2DsRed pericyte ramification was observed. Arrowheads indicate pericyte soma. Adapted with permission from Milesi et al (2014). (C) Integrity of cortical blood vessel tight junctions is impaired at late but not early time points after transient MCAO in live Tg eGFP-Claudin5 mice. Maximum intensity projections of 120-μm-thick cortical volumes from healthy mouse brain, 12–14 hr, 24–30 hr, and 48–58 hr after reperfusion obtained with two-photon imaging through a cranial window in a stroke core region. Scale bar = 50 μm. Adapted with permission from Knowland et al (2014).

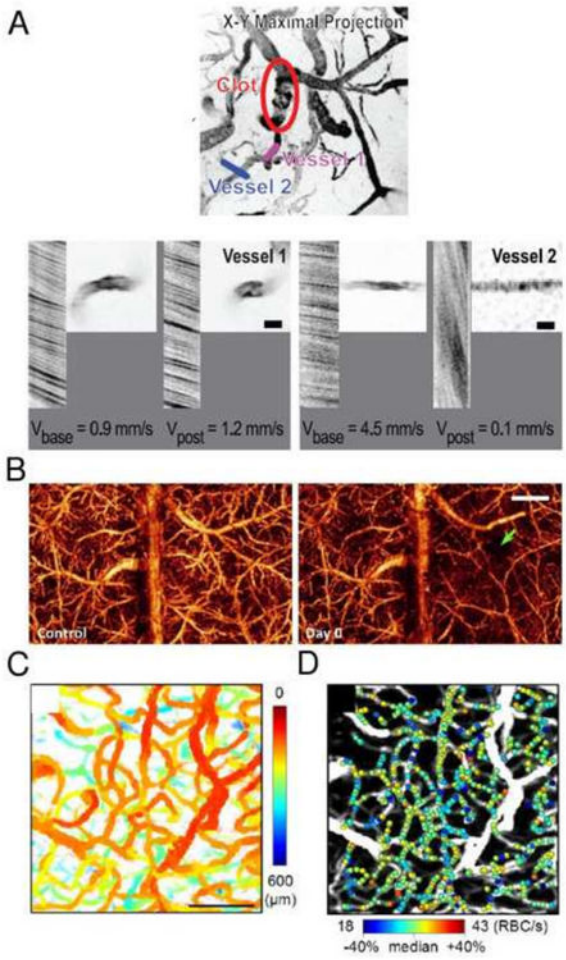

Fig. 4.

Imaging of cerebral blood flow. (A) MPM images of blood flow redistribution in vessels in the immediate neighborhood of the clot in the penetrating arteriole in rat somatosensory cortex. The line segments indicate specific microvessels whose velocity and spatial profile were measured before and after the occlusion. High magnification images and line-scan data for indicated vessels are shown before and after induction of a clot. For the latter data, the nonfluorescent RBCs appear as dark streaks on a bright background; the sign and magnitude of the slope of the streaks reflects the direction and speed, respectively, of RBC motion. Adapted with permission from Nishimura *et al* (2007). (B) Label-free OCT imaging of blood flow. 3D optical microangiography (OMAG) imaging of the mouse cortex between anterior and posterior coronal sutures *in vivo* at baseline and after traumatic brain injury (TBI). The site of injury is pointed by the green arrow. The scale bar = 1.0 mm. Adapted with permission from Jia *et al* (2009). (C, D) OCT imaging of RBC flux in cortical capillaries. (C) The enface MIP of the 3D OCT angiogram of rat somatosensory cortex with color indicating the depth from the cortical surface. Scale bar = 100 μm. (D) Estimated RBC flux obtained by analyzing individual RBC passage in time-series OCT data from (C), presented as color spots on the MIP angiogram. Adapted with permission from Lee *et al* (2013b).

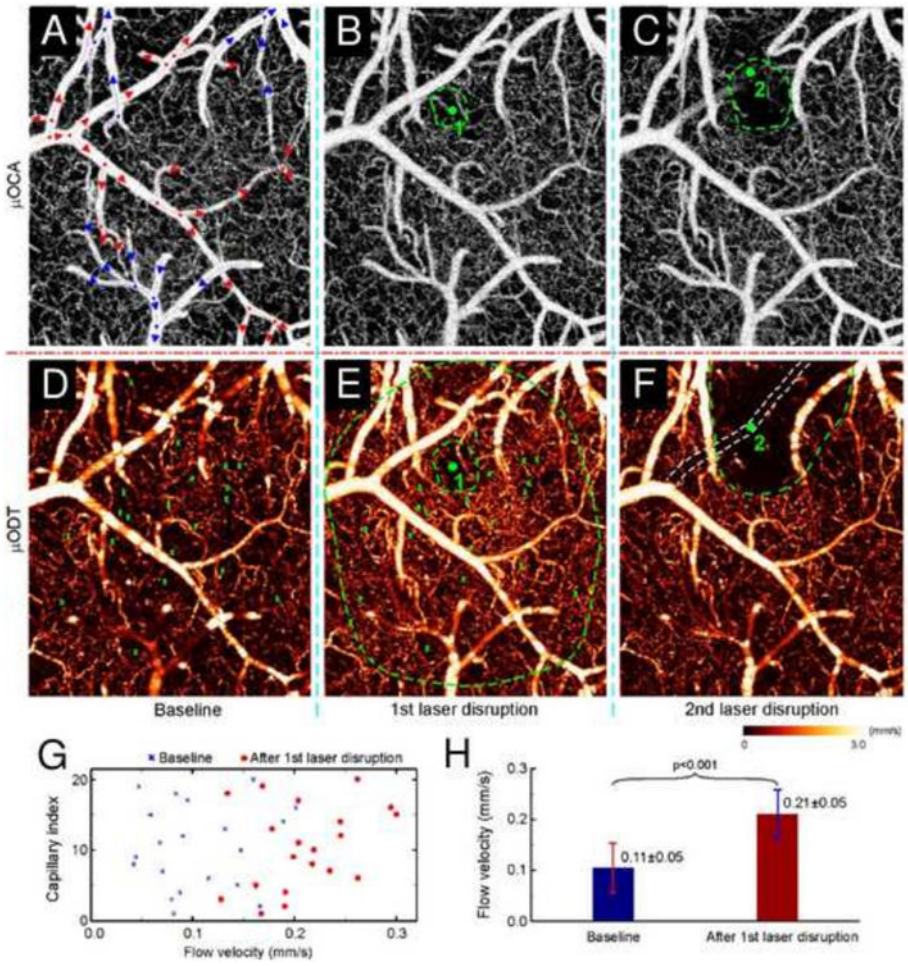

Fig. 5.

OCT imaging of laser disruptions of a cerebral capillary (1) and a branch vessel (2) in mouse cortex. Upper panel: maximum intensity projection (MIP) images of microvasculature (optical coherence angiography) at baseline (A), after laser disruption of a 9 mm wide capillary (B) and of a 35.8 mm wide arteriole (C). Red/blue arrows: flow directions in arterioles and venules; dots: vessel junctures. Lower panel: MIP images of cerebral blood flow (CBF; microvascular imaging by optical Doppler tomography) at baseline (D) and after laser disruptions (E, F). Angiography detects no difference except reduced vasculature in the immediate areas (dashed green circles in panels B and C) around laser disruption (green dots); whereas quantitative CBF reveals vastly expanded vasodilatation almost over the entire field after laser disruption of a capillary (dashed outer green circle in panel E) and the quenching of local CBF networks over a much larger area (dashed green circle in panel E). Quantitative comparisons among 20 capillaries indicate that CBF increased significantly from 0.105 ± 0.049 mm s^{-1} at baseline to 0.211 ± 0.048 mm s^{-1} at 30 min after laser disruption (G and H; $P < 0.001$). Image size: 1×1.2×1 mm^3. Laser radiation: 532 nm per 60 mW, ∼3 μm wide focal spot; 2 and 6 min exposures for capillary (1) and arteriole (2), respectively. Adapted with permission from Ren *et al.* (2012).

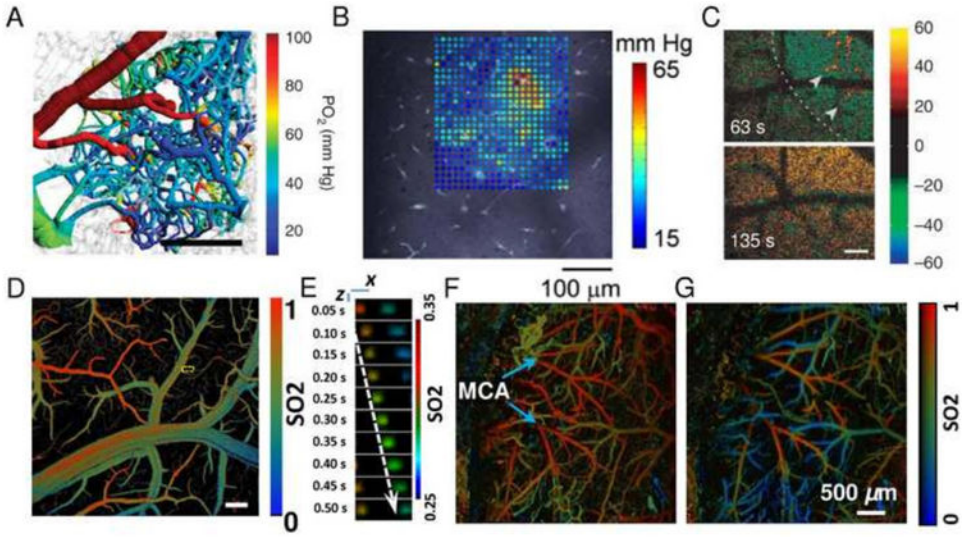

Fig. 6.

Imaging of PO2, SO2, and NADH. (A) Mouse cortical microvascular PO2 measurements using PLIO2 overlaid over microvascular structures. Scale bar = 200 µm. Adapted with permission from Sakadzic et al (2014). (B) A grid of intravascular and tissue PO2 values measured by PLIO2 in a rat somatosensory cortex superimposed on the vascular reference image. Adapted with permission from Devor et al (2011). (C) MPM imaging of relative NADH fluorescence intensity changes (colorbar) during cortical spreading depression in mouse cortex 50 µm below the cortical surface. Decreases (dips) are displayed in green-blue and NADH increases (overshoot) in red-yellow. Dashed lines indicate the wave front moving across the field. Arrowheads indicate areas with NADH overshoot. Scale bar = 100 µm. Adapted with permission from Takano et al (2007). (D, E) Single cell label-free photoacoustic microscopy of oxygen metabolism *in vivo.* (D) SO2 mapping of the brain vasculature using photoacoustic microscopy. Scale bar = 200 µm. (E) Single cell oxygen unloading along a capillary marked with the yellow dashed box in (D). The dashed arrow follows the trajectory of a single flowing RBC. Scale bar = 10 µm. Adapted with permission from Wang et al (2013). (F,G) Transcranial photoacoustic microscopy imaging of cerebral microvascular SO2 in mice before (F) and during MCA occlusion (G). Adapted with permission from Hu et al (2011).

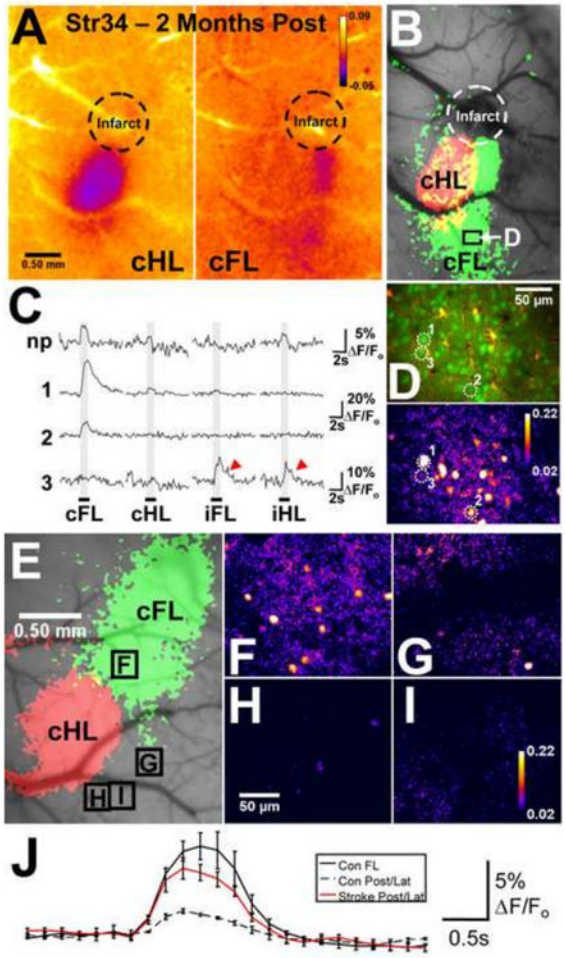

Fig. 7.

Posterior S1 forelimb (S1FL) reorganization. (A) and (B) Mouse Strain 34, imaged 2 months after photothrombosis: IOS response maps show increased overlap between the contralateral FL (cFL) - and contralateral hind limb (cHL)-evoked IOSs, and a posterior shift in cFL activation. (C) Ca^{2+} imaging (depth, 141 µm, from the labeled region in the IOS map) demonstrated that the posterior regions of the reorganized cFL representation contained neurons (e.g., 1, 2, labeled in (D)) with strong, limb-selective responses to cFL stimulation. Aberrant responses (red arrowheads) were observed in some neurons (e.g., 3). (D) A difference image illustrating the strong Ca^{2+} -induced fluorescence signal (F/F_o) over 3 s after cFL stimulation onset in the image section from which the representative neurons in (C) were selected [shown below the corresponding 2-photon image of OGB-1 (green) and SR101 (red) labeling]. (E) IOS maps from a naive animal showing the cFL- and cHL-evoked representations. (F)–(I), Difference images illustrating the F/F_o in S1FL and regions of the cortex posterior to S1FL and lateral/posterior to S1HL during cFL stimulation (over 3 s after stimulus onset) from the mouse shown in (E) (borders of the image sections denoted on the IOS map in (E)). Importantly, cFL stimulation evoked little or no Ca^{2+} signal in the posterior and lateral regions in control animals. (J) Mean records of the Ca^{2+} image field activity elicited by cFL stimulation in the S1FL (n=2*) and posterior/lateral (Post/Lat) cortex (n=4) of control mice and the same regions in animals imaged 1–2 months after

stroke (n=7). The cFL-evoked activity revealed by two-photon Ca^{2+} imaging in these posterior and lateral regions was significantly stronger in stroke animals compared with controls (ANOVA, $p<0.009$), confirming the posterior S1FL reorganization suggested by the IOS maps. *In two mice, OGB-1 AM was microinjected in S1FL and the control regions posterior and lateral to S1FL/S1HL, whereas it was injected into S1HL and the control regions in two other controls. Adapted with permission from Winship and Murphy (2008).

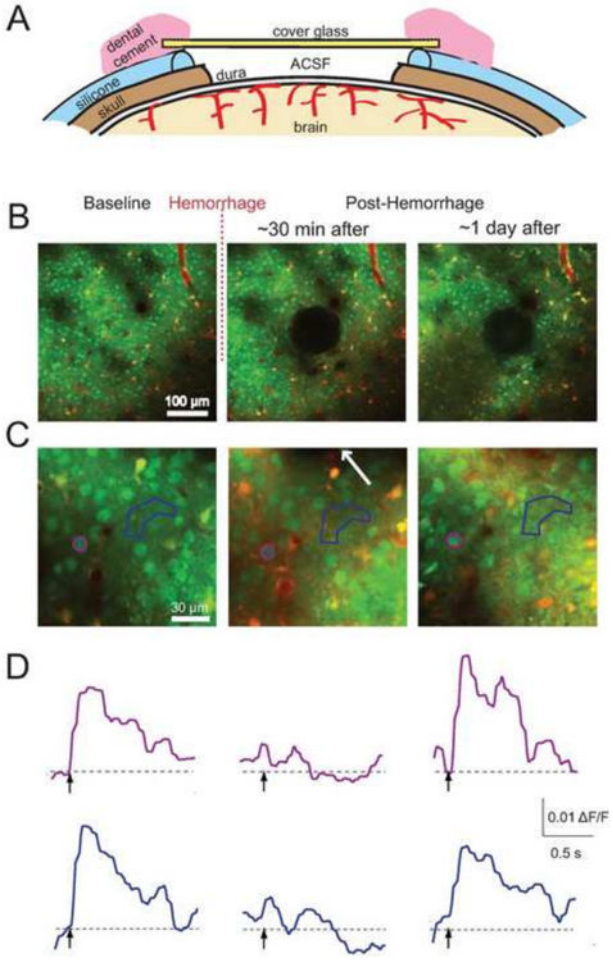

Fig. 8.

Chronic imaging of stimulus-induced calcium transients after a microhemorrhage. (A) Schematic of a re-openable chronic cranial window preparation for mouse. A layer of silicone coated the skull around the craniotomy, and the glass was glued to the silicone. The window was reopened by gently detaching the silicone from the skull, enabling reinjection of OGB and sulforhodamine 101 into the cortex. (B) Low- and (C) high-magnification 2PEF images of the same regions of the brain before, immediately after, and one day after inducing a microhemorrhage. The hematoma is visible in the center of the second and third panels in (B). The arrow in the second panel of (C) indicates the direction to the microhemorrhage, located 40 µm away. (D) Stimulus-induced calcium responses from the neuronal cell body and region of neuropil indicated on panel (C) by color coding. Adapted with permission from Cianchetti et al. (2013).